Recent Progress for Hydrogen Production from Ammonia and Hydrous Hydrazine Decomposition: A Review on Heterogeneous Catalysts

Panayiota Adamou[1], Silvio Bellomi[2], Sanaa Hafeez[3], Eleana Harkou[1], S.M. Al-Salem[4], Alberto Villa[2], Nikolaos Dimitratos[5,6], George Manos[3] and Achilleas Constantinou[1]*

1. Department of Chemical Engineering Cyprus University of Technology, 57 Corner of Athinon and Anexartisias, 3036 Limassol, Cyprus.
2. Dipartimento di Chimica, Universitá degli Studi di Milano, via Golgi, 20133 Milan, Italy.
3. Department of Chemical Engineering, University College London, London WCIE 7JE, UK.
4. Environment & Life Sciences Research Centre, Kuwait Institute for Scientific Research, P.O. Box: 24885, Safat 13109, Kuwait.
5. Dipartimento di Chimica Industriale "Toso Montanari", Alma Mater Studiorum Università di Bologna, Viale Risorgimento 4, Bologna 40136, Italy.
6. Center for Chemical Catalysis-C3, Alma Mater Studiorum Università di Bologna, Viale Risorgimento 4, Bologna 40136, Italy.

* Author for correspondence: a.konstantinou@cut.ac.cy;

Abstract

In response to the growing trend of greenhouse gas emissions from the production and use of conventional fuels, CO_x free hydrogen generation is introduced as an alternative and efficient energy carrier. Due to hydrogen's storage challenges, is more efficient to be produced *on-site* by other chemical compounds for fuel cell applications. This work outlines the production of hydrogen (H_2) from ammonia (NH_3) and hydrous hydrazine ($N_2H_4.H_2O$) catalytic decomposition. Both substances are giving nitrogen (N_2) as a by-product, which is not toxic. Moreover, heterogeneous catalysts that were studied through the years are presented. Lastly, a reactoristic view of the ammonia decomposition is provided with different reactors such as catalytic membrane reactors (CMRs), fixed-bed reactors (FBRs) and micro-reactors (MRs) for the evaluation of their performance.

Keywords: Ammonia, Hydrous Hydrazine, Hydrogen, Catalysts, Reactors

1 Introduction

Environmental concerns are increasing as the extensive use of fossil fuels in the energy sector is the biggest contributor to climate change. Fossil fuels undergo the process of combustion to release their energy content, polluting the atmosphere with emissions of greenhouse gases (GHGs) and harmful substances. These resources are non-renewable and are not evenly distributed around the world [1]. There is an increasing urge in recent years to find and adopt alternative emission-free energy sources in hope to stabilise the negative impacts conventional fuels have created in the environment. Hydrogen (H_2) is preferred as an energy carrier due to its zero emissions during combustion and its generation from various paths such as non-renewable sources, biomass and water electrolysis [2].

Hydrogen can be produced by either from fossil fuels, capturing carbon emissions or renewable resources. Depending on the material, H_2 can be classified as grey, blue, and green respectively. Two of the common methods to produce H_2 is steam methane reforming and water splitting reactions such as water electrolysis [3–6]. Fuel cells then can be used to convert H_2 into power through the electrochemical reaction that follows (Eq. 1):

$$2H_2 + O_2 \rightarrow 2H_2O + \text{Energy} \quad (1)$$

Eq. 1 shows H_2 reaction with oxygen to produce water and energy in the form of electricity or heat as the inverse reaction of electrolysis. Fuel cells are very promising and are already used in various stationary and mobile applications such as back-up power supplies, road vehicles, as well as rockets and space shuttles. The main concept revolves around generating green energy which is considered revolutionary [7]. However, its storage and transportation problems have not yet reached an applicable level for further industrial use.

Ammonia (NH_3), among other H_2 energy sources, is a promising alternative. It is mainly produced from the decomposition of urea and other nitrogen compounds during wastewater treatment processes or from the microbial decomposition of organic substances containing nitrogen [8]. It possesses high H_2 content (17.8 wt %) and a large energy density (3000 Wh/kg). It has greater volumetric hydrogen density than liquid H_2 (121 kg H_2/m^3) and can be liquefied and stored at room temperature facilitating transportation and storage [9–12]. Furthermore, the decomposition of ammonia is CO_x-free producing only H_2 and nitrogen (N_2) (Eq. 2) [13].

$$NH_3 \rightleftharpoons \frac{1}{2} N_2 + \frac{3}{2} H_2 \quad (2)$$

Ramsay and Young [14] were the first to study the temperature at which ammonia decomposition takes place and the influence of the vessel or tube material that contains the gas in the early 1880s. Then at the beginning of the 20th century Perman and Atkinson [15] studied both the effect of temperature and pressure on the rate of decomposition as well as the catalytic activity of Hg, Fe, and Pt.

Hydrous hydrazine ($N_2H_4.H_2O$) has also been proposed as a promising candidate for H_2 generation. It can be produced by the Raschig process that involves the ammonolysis of hypochlorite to hydrazine and ammonia or the oxidation of anhydrous ammonia by chlorine [16]. Hydrous hydrazine has a high hydrogen content (8.0 wt %) and due to its carbon-free content, the generation of H_2 has zero emissions [17–20]. The products from hydrazine decomposition are H_2 and N_2; however, an undesirable side reaction of incomplete decomposition may occur producing ammonia, which must be avoided because it reduces the efficiency of the H_2 generation process. The two reaction pathways for hydrazine decomposition are depicted in Eqs. (3-4) [21].

$$H_2NNH_2 \rightarrow N_2 + 2H_2 \quad (3)$$

$$3H_2NNH_2 \rightarrow 4NH_3 + N_2 \quad (4)$$

This review will highlight H_2 storage challenges and the generation of H_2 from ammonia and hydrous hydrazine. Moreover, the heterogeneous catalysts for the decomposition of the substances mentioned above and the structural properties of the catalysts, will be addressed. Furthermore, different types of reactors that have been applied for the ammonia decomposition, will be covered to provide an overview of the most innovative and efficient future systems. Regarding hydrous hydrazine, there are not many studies in the development and design of reactors and therefore, reactor set-ups will be not discussed.

2 Hydrogen Storage Challenges

Although H_2 offers an attractive and promising solution as an alternative energy carrier, its storage and transportation are one of the main technical barriers preventing H_2 for wider applications. This is due to hydrogen's very low density of 0.089 kg/m^3 at 0 ^{o}C and 1 bar. At ambient temperatures and 1 atm pressure, 1 kg of H_2 occupies 11 m^3, which results in a large volume required for storage. Nonetheless, H_2 is extremely flammable with a flame speed nearly

an order of magnitude higher than gasoline when mixed with air, therefore, its safety issues must be resolved [22].

Due to the lack of appropriate infrastructure for storage, transportation and distribution of H_2, new methods must be found to store it safely. For large scale and long-term storage, different underground storage sites were proposed such as salt caverns, aquifer formations or depleted oil and gas fields. Salt caverns are currently the most favorable method. No in-situ reactions either with microorganisms or any chemical elements occurred so far and the leakage rates are very low because salt caverns exhibit the required tightness. In contrast with aquifer formations or depleted oil and gas fields that occur naturally, salt caverns need to be developed in an already existing underground salt formations, so not all regions have the necessary geological characteristics [23].

Moreover, it is necessary to increase the volumetric energy (density) of H_2 which can happen either by liquefying it or by compressing it. Pressurised tanks can take the form of cylindrical or spherical vessels or bottles, and while raising the pressure, gaseous H_2 density increases achieving higher storage density. These are currently used in stationary applications mainly to store hydrogen in hydrogen refuelling stations [24]. Their cost may differ from the material used and the pressure applied in the tank. On the other hand, cryogenic tanks store liquefied hydrogen at -253 ^{o}C (atmospheric pressure) because the liquefaction process increases H_2 volumetric density drastically. These are not designed to withstand high pressures inside, hence they must be isolated to reduce as much as possible heat transfer. However, compressing requires high pressures and liquefying needs extremely low temperatures such as -253 ^{o}C that can only be achieved with multiple heat exchangers and a combination of multiple cooling cycles [25].

New technologies such as metal hydrides and carbon nanotubes are gaining attention for their H_2 storage properties. Metal hydrides can store H_2 due to their large storage capacity at ambient pressure and temperature. Hydrogen reacts with metals which have the ability to absorb and desorb it by breaking or bonding the chemical bonds making them an efficient form of hydrogen storage [26]. Adsorption of H_2 in carbon nanostructures is an attractive solution for hydrogen storage due to the high surface area of carbon. There are a variety of carbon materials, such as single walled carbon nanotubes (SWCNTs), multiwalled carbon nanotubes (MWCNTs) and carbon nanofibers (CNFs). However due to some controversial results that were obtained from some studies regarding the H_2 adsorption measurements, much research is still needed for

their efficient usage [27]. For example, in the late 1990s, Dillon et al. [28] suggested that SWCNTs have a very high H_2 uptake up to 5-10 %. Moreover, Chambers et al. [29] published an even more extraordinary result. It was claimed that the hydrogen storage capacity of graphite nanofibers (GNFs) materials was up to 67.6 %. Both of these results were questionable thus research groups [30–32] tried to reproduce and validate the results without success since the capacity of the materials was very much lower.

3 Hydrogen Production Routes

Various raw materials can be utilised to produce H_2 following different production routes. Given the raw material, H_2 can be colour coded as black, grey, blue or green.

In spite of the growing number of studies focusing on renewable hydrogen production, fossil fuel-based hydrogen generation is still being examined. Black or brown H_2 is produced from coal through the process of gasification. It is considered a very environmentally damaging method as carbon dioxide and carbon monoxide are also generated and emitted in the atmosphere. Liu et al. [33] investigated the gasification mechanism and developed a coal supercritical water gasification reaction kinetic model taking into consideration the migration mechanism of nitrogen and sulfur. The model could not only predict the generation of hydrogen, carbon monoxide and carbon dioxide but ammonia and hydrogen sulfide as well, proving the interaction between hydrocarbon gas and the gasification products of nitrogen and sulfur.

H_2 is labelled grey when extracted from natural gas via steam-methane reforming. It is the most common form nowadays with over 95 % of the global hydrogen production coming from reforming of conventional fuels and around 50 % of that is generated from steam reforming of natural gas [4]. Steam methane reforming (SMR) is an endothermic reaction (600-700 ^{o}C) and the catalysts mostly used for this reaction are nickel-based. Ngo et al. [34] utilised a SMR unit with a furnace and a reactor, where the furnace produces heat via the natural gas reaction with oxygen and the reactor consumes heat and generates H_2. Another study conducted by Cho et al. [35] used facility-level data to examine the pollutant emissions which may differ from the theoretical estimates due to various process conditions and types of pollution controlled equipment. Direct emissions from 33 facilities used were 9.35 kg CO_2/kg H_2 and increased up

to 11.2 kg CO_2/kg H_2 when the full cycle of H_2 production was included. Increasing 10 % in hydrogen production efficiency the global warming impact can be reduced up to 11.1 %.

Blue H_2 is produced from fossil fuels like black and grey H_2 but the carbon generated from the process is captured. It can be described with the term carbon neutral but low-carbon H_2 would be a more appropriate term since not all carbon emissions are captured. Even though CO_2 can be captured by absorbents or amine solvents, it must be stored after, which is costly. Therefore Khan et al. [36] explored the possibility to use the carbon captured by converting into formic acid by the electrode-reduction. An amine-based CO_2 capture unit was utilised with 90 % capture efficiency. The carbon could either be stored or utilised. It was concluded that by utilising it instead of storing it, is more cost-effective and is a promising approach for further future work.

Lastly, green H_2 uses renewable sources such as biomass, geothermal, wind and solar energy [37]. Biomass feedstock such as agricultural crop residues, food and municipal waste can produce hydrogen carrier compounds through the process of fermentation, hydrolysis, or oxidation. Formic acid, an organic hydrogen carrier, is considered as one of the main products derived from biomass. The catalytic decomposition of formic acid is well investigated because of its properties as an excellent hydrogen source. Hafeez and Sanchez et al. [38] utilised a Pd/C catalyst for the decomposition of formic acid in a packed bed microreactor. The validation of experimental data was confirmed by the development of a CFD model. Moreover, the deactivation of the catalyst was accurately depicted by the model promoting the use of the model to predict the formic acid decomposition. Another study by Hafeez et al. [39] investigated the use of a 2%Pd_6Zn_4 catalyst in a batch reactor for the decomposition of formic acid and a process-simulation model gave a good validation of the experimental data. The catalyst was studied in a temperature range of 30-60 ^oC and with different concentrations (0.1-0.5 M), where in both cases no loss of activity was observed. The dehydrogenation of hydrogen carrier compounds with zero CO_2 emissions is an alternative solution to formic acid and will be discussed later. Another common method used to obtain green H_2 is water splitting reactions such as electrolysis of water. Water reacts at the cell's anode and under the influence of current it decomposes and produces O_2 at the anode of the cell and finally H_2 at the cathode [40].

Apart from these, H_2 can be classified to turquoise, pink, yellow and white which are not commonly used. Turquoise refers to H_2 produced from methane pyrolysis with solid carbon as a by-product. Even though methane pyrolysis is not a sustainable process since natural gas reserves are depleting, it can provide a temporary solution until renewable technologies are fully developed. The process begins with the cracking of methane to H_2 and solid carbon, then the removal of the carbon from the stream and lastly, the purification of the gas stream. High temperatures are needed for methane pyrolysis, up to 1000 ^oC for non-catalytic systems. Suitable catalysts such as nickel, iron, and carbon have been extensively studied and the decomposition of methane can be triggered at lower temperatures (500-800 ^oC) [41].

Pink (or purple) and yellow H_2 are both produced through electrolysis using nuclear power and solar power respectively [42]. The difference from conventional electrolysis to nuclear high temperature electrolysis (HTE), is that the later uses heat from nuclear power plants to moderate electricity consumed for electrolysis. In general, nuclear HTE occurs at 800-1000 ^oC and an yttria-stabilised zirconia is used as an electrolyte [43]. A solar-based electrolysis consists of a concentrating collector, a heat engine, an electrical generator, and electrolyser. A part of the absorbed solar radiation is converted to mechanical work and then the electrical generator transforms it to electrical power. Then, the generated electricity is used to electrolyse water and produce H_2 and O_2 [44].

White H_2 refers to the by-product obtained from industrial processes such as catalytic thermochemical splitting of water, or it may be referred as its natural occurring form. The thermochemical splitting occurs without intermediate step and is based on the use of concentrated solar energy. This pathway may further reduce economic and environmental costs [45].

Potential applications of H_2 after its production are its use as an industrial feedstock, power generation, stationary and transportation [46]. Fig. 1 summarises the H_2 colour spectrum according to the feedstock and production used.

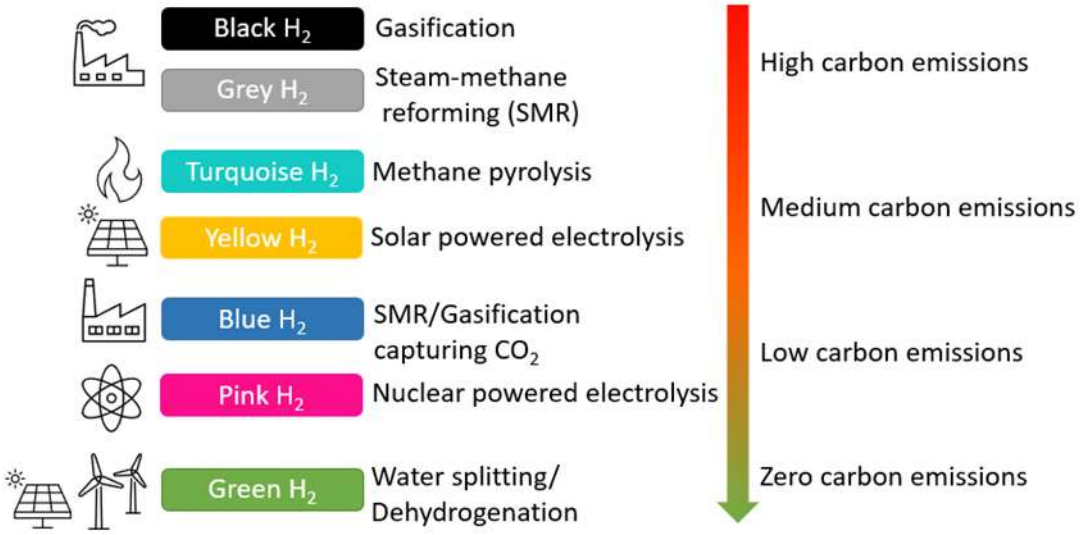

214 Fig. 1. Hydrogen colour spectrum.

215

216 # 4 Ammonia Decomposition as a sustainable hydrogen production method

217 ## 4.1 Heterogeneous Catalysis of Ammonia Decomposition

218 Heterogeneous catalysis can be described as the catalysis whereas the phase of the catalyst is
219 different from the phase of the reactants/products. Thus, heterogeneous catalysts are, mostly,
220 in the solid state while the reactant mixture is either liquid or gas, in contrast with homogeneous
221 catalysts that exist in the same phase with the mixture. Heterogeneous catalysts have the ability
222 to regenerate, separate easily from the products, shaped into different geometries and give high
223 rates [47]. Table 1 summarises the most effective heterogeneous catalysts utilized for the
224 decomposition of ammonia.

Since the 19th century, ammonia decomposition has been investigated mostly to understand the ammonia synthesis with the presence or absence of catalysts. Over the last decade, the catalytic decomposition of ammonia has gained a lot of attention and catalysts such as platinum (Pt) [48], palladium (Pd) [49], ruthenium (Ru) [50] and, rhodium (Rh) [51] that were known to catalyse ammonia synthesis have been used in different experiments [52]. Ru was found to be the most active and studied catalyst as there is a plethora of studies according to Ru-based catalysts [53–57]. Unfortunately, the large scale of application of Ru catalysts is not cost effective and their limited availability leads to the necessary development of cheaper catalytic systems with the same efficacy. The production steps of H_2 by ammonia are depicted in Fig. 2.

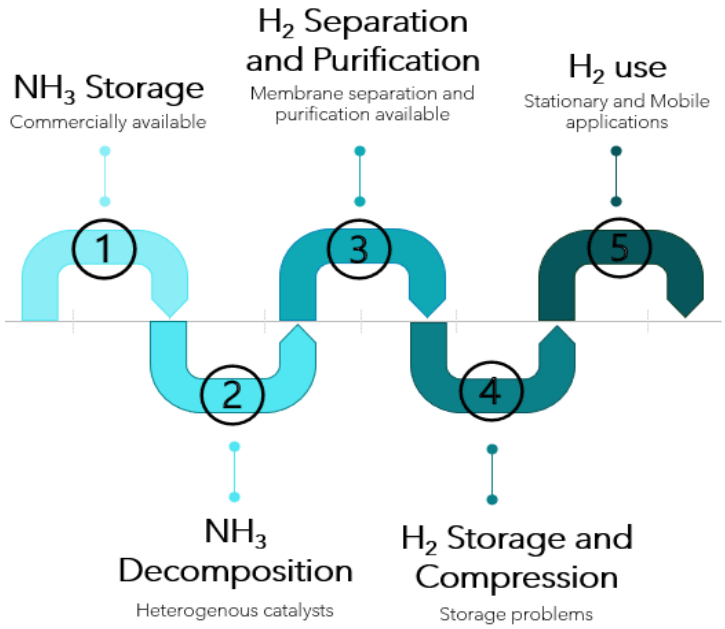

Fig. 2. Production steps of hydrogen by ammonia [12].

Ni metal particles were used as catalysts with $MgAl_2O_4$ as supports by Qiu et al. [58] for investigation of the support effect on the catalytic decomposition of ammonia. From the catalysts tested $Ni/MgAl_2O_4$ – LDH, developed by hydrothermal synthesis, had the best catalytic activity with 88.7 % NH_3 conversion and a H_2 production rate of 1782.6 mmol g_{cat}^{-1} h^{-1} at 600 ^oC with a stable performance for a period of 30 h. $Ni/MgAl_2O_4$ – LDH catalyst had the highest surface area (148.3 m^2/g) and therefore it resulted in high Ni dispersion (29.6 %) enhancing the NH_3 conversion and weakening the H_2 poisoning. $Ni/MgAl_2O_4$ – LDH catalyst was further examined for its stability at a temperature range of 550-650 ^oC for 24 h and the results showed that the catalyst was highly stable due to the strong metal-support interactions.

It was concluded that this catalyst with high stability, activity, and low cost it is essential to be developed more and used in upscale application for H_2 generation.

Cobalt particles supported on carbon doped with nitrogen were prepared via pyrolysis of ZIF-67 at a range of temperatures (Co/NC-X, X = 500, 600, 700 and 800 ^oC) by Li et al. [59]. The synthesis process of the catalysts resulted in an evenly dispersion of the Co particles hindering their aggregation. At temperatures below 300 ^oC the catalysts were inactive. While increasing the temperature the conversion of ammonia increased and the best catalytic activity was obtained by Co/NC-600 with an NH_3 conversion of 80 % and H_2 production rate of 26.8 mmol H_2 g_{cat}^{-1} min^{-1} at 500 ^oC and hardly decreased even after 72 h. The bond strength between the metal and nitrogen, according to previous studies, plays a key role in the decomposition of ammonia. If the bond is either too weak or too strong it affects the adsorption of NH_3 and the desorption of the intermediate products resulting in a low catalytic activity. Thus, medium metal-nitrogen bond strength is required for this reaction and from further investigation it was found that the Co-N bond energy of Co/NC-600 catalyst is in the middle range and thus acting beneficial for the reaction.

Ru particles supported on $SmCeO_x$ were investigated by Tang et al. [60] for evaluation of the effect of the Sm doping to the catalysts. At 400 ^oC, the Ru/$SmCeO_x$ catalyst, with 1.4 nm average particle size, obtained a conversion rate of 74.9 % corresponding to a H_2 production rate of 161.1 mmol g_{Ru}^{-1} min^{-1}, much higher than other supports with Ru particles tested for this catalytic reaction. Characterisation techniques were used to study the properties and structure of the Ru/$SmCeO_x$ catalyst. The high activity was attributed to the doping of Sm that formed in plenty of oxygen vacancies which have strong interaction with Ru resulting in a high Ru dispersion.

A series of Co_3O_4 catalysts supported on barium hexaaluminate (BHA) with various mass loadings of Co (XCo/BHA, X = 10 %, 20 %, 30 %, 35 % and 40 %) and 0.5 g BHA were prepared by Li et al. [61]. BHA alone was inactive and with an increase of Co loading the activity also increased. The 35Co/BHA catalyst demonstrated the highest catalytic activity among the others with a conversion rate of 87.2 % at 500 ^oC and a H_2 production rate of 29.2 mmol H_2 $gcat^{-1}$ min^{-1}. After 200 h the conversion rate was at 85 % indicating the catalysts great stability.

Ru-based catalysts supported on reduced graphene oxide were developed by Pinzón et al. [62] for hydrogen generation by ammonia decomposition. The effect of the Ru loading as well as

the effect of the amount of the support material were examined. With a content of Ru up to 2.5 wt %, an increase in the catalytic activity was noticed (92 %), while Ru loading higher than 2.5 wt % resulted in agglomeration decreasing the number of active sites and therefore the ammonia conversion. With the addition of the pre-reducing agent the catalytic activity increased. The optimal catalytic activity was observed from 2.5Ru/10C-rGO catalyst with a conversion of 96 % and H_2 production rate of 349.7 mmol H_2 g_{Ru}^{-1} min^{-1}. After 60 h of reaction the catalyst did not show any significant change in its performance.

In an attempt to imitate the activity of the Ru catalysts, Kirste et al. [63] developed alloys of different unsupported bimetallic catalysts ($CoRe_{1.6}$, Ni_2Mo_3N and Co_3Mo_3N) for the on-demand production of H_2 via ammonia decomposition. In parallel, 7 wt % Ru/CNTs catalytic particles were also synthesized to compare the catalytic activities. $CoRe_{1.6}$ obtained a similar activity with Ru/CNTs due to the alloy synergistic effect. The catalyst was pre-reduced at a temperature range of 400-600 ^oC, which had a major impact on the catalytic performance with an increase of the temperature. At 500 ^oC reaction temperature and 600 ^oC reduction temperature, NH_3 conversion was above 90 % and after 6 consecutive runs $CoRe_{1.6}$ presented excellent stability with no significant changes in the structure except the partial oxidation and re-reduction of the Co particles that acts in favour on the restart of the NH_3 decomposition.

Potassium promoted iron catalysts supported on carbon (K^+-Fe/C) were studied by Jedynak et al. [64] to show the influence of the iron particle sizes on the rate of ammonia decomposition. Results showed that smaller particles gave higher TOFs in contrast with larger particles. K^+-Fe5.7/C (12.5 nm) gave a TOF value of 0.5 s^{-1} in contrast with the K^+-Fe24/C (24 nm) that displayed a TOF value of 0.25 s^{-1} concluding, that the smaller the surface of iron crystallites is, the more advantageous are the catalytic properties.

Ganley et al. [65] examined 13 metallic catalysts (Ru, Ni, Rh, Co, Ir, Fe, Pt, Cr, Pd, Cu, Te, Se, Pb) supported on pellets of activated alumina in order to suggest potential alternatives of Ru catalysts due to their high cost. Ru was the most active catalyst and besides Ni that had 40% lower activity than Ru, all the others were not efficient for the ammonia decomposition reaction. Also, depending on the catalyst that is used, the rate limiting step differs regarding nitrogen desorption or N-H bond scission. This suggests that is unlikely to predict catalytic behaviour using only one parameter by assuming that a range of metallic catalysts have the same rate determining step for a given reaction.

Carbon nanotubes (CNTs) with residual Co or Fe nanoparticles were used as catalysts by Zhang et al. [66] for ammonia decomposition. With an increase in the temperature, ammonia conversion also increased and even at higher temperatures such as 700 ^{o}C the chemical composition and microstructure of CNTs remained the same as it was before the reaction took place. Fe containing CNTs had an activation period of 1200 min with a conversion up to 76 % but Co containing CNTs showed the highest activity overall with a conversion almost up to 100 %. The higher activity of Co-containing CNTs might be due to their smaller particle size (4-20 nm) when compared with Fe-containing particles that were in the range of 10-50 nm, and the capacity of CNTs as electron reservoirs.

El-Shafie et al. [67] developed zeolite (SA-600A)-based catalysts with Ru and Li as supporting materials at different mixing ratios for H_2 generation from ammonia decomposition. For all the developed catalysts it was observed that increasing the temperature the conversion rate increased as well. It was observed that the catalyst was enhanced when the Li mixing ratio was increased, and the highest NH_3 conversion rate (99.9 %) was obtained from the catalyst with a Li mixing ratio of 4 %. The increase of Ru ratio enhanced the conversion rate even more at lower temperatures. The catalyst with mixing ratio of 40 g (SA-600A)/5 g $RuCl_3.nH_2O$/3 g $LiOH{\cdot}H_2O$ obtained the highest catalytic activity and NH_3 conversion of 99.9 % at 490 ^{o}C.

Core-shell iron-based catalysts (α-FeO_2O_3-x@$pSiO_2$) were synthesized for ammonia decomposition by Feyen et al. [68]. The catalysts were found to be highly stable up to temperatures of 800 ^{o}C with higher reaction rates and full conversion for all the tested catalysts. Moreover, particle sizes between 35 and 75 mm showed a limited influence on the catalytic activity. Lastly, there were no diffusion limitations up to flow rates of 120000 $cm^3\,g_{cat}^{-1}\,h^{-1}$ that could have been observed from the porous silica shells.

Cobalt catalysts supported on different carbon materials were developed for H_2 production from ammonia decomposition by Zhang et al. [69]. The carbon materials that were utilised for the research were multi-walled carbon nanotubes (MWCNTs), single wall carbon nanotube (SWCNTs), three types of activated carbons (AC) and reduced graphene oxides (RGO). The highest NH_3 conversion was conducted by the Co/MWCNTs catalyst. The conversion of Co/RGO and Co/SWCNTs catalysts was very low and therefore they weren't used for further studies. Moreover, the influence of post-treatment temperature on the catalytic performance of 10Co/MWCNTs (10% wt Co) was evaluated in this study at a temperature range of 230-700 ^{o}C. Highest TOF value was obtained at 600 ^{o}C and it reached up to 8.15 s^{-1}. Even after 20 h of

catalytic test there was no significant change in the mean particle size of Co. The fresh catalyst had a mean particle size of 4.8 nm while the used catalyst had a mean particle size of 5.6 nm. Due to its higher catalytic stability and the excellent catalytic activity for the decomposition of ammonia, Co/MWCNTs catalyst could be promising for future applications.

Catalysts with 2 % Ru content supported on lanthania-ceria materials with different molar ratios were synthesized by Le et al. [70] to evaluate the H_2 production by ammonia decomposition. The catalytic activity was tested at temperature range of 300-500 ^oC and the $Ru/La_{0.33}Ce_{0.67}$ exhibited the best catalytic performance with an ammonia conversion of 91.9 % and H_2 formation rate of 6.2 mmol g_{cat}^{-1} min^{-1}. The acid-base properties of the $La_xCe_{1-x}O_y$ supports combined with the high dispersion of Ru particles resulted in the enhanced catalytic activity. After 100 h the catalyst maintained its high catalytic activity due to its excellent stability, since fresh and used catalyst had a mean particle size of 3.3 nm and 3.6 nm respectively, showing no significant difference in the size and structural morphology of the particle.

Monometallic Ni, Co and bimetallic Ni-Co alloy catalysts supported on SiO_2 were prepared by a co-impregnation method by Wu et al [71]. Bimetallic catalysts had better catalytic performance obtaining higher ammonia conversion due to the alloy synergistic effect between Ni and Co. Among the tested catalysts, the Ni_5Co_5/SiO_2 exhibited the highest catalytic activity achieving 76.8 % NH_3 conversion and H_2 formation rate of 25.71 mmol g^{-1}_{cat} min^{-1} under GHSV of 30,000 mL h^{-1} g^{-1}_{cat} at 550 ^oC. The effect of GHSV was also examined showing that the increase of GHSV resulted the conversion decrease. With lower GHSV of 6000 mL h^{-1} g^{-1}_{cat} the catalyst achieved 94.7 % NH_3 conversion. Further enhancement on the conversion (78.1 %) was observed when K was added during the Ni_5Co_5/SiO_2 synthesis (K/(Ni + Co) molar ratio of 1:10) indicating that alkali act in favour of the catalytic decomposition of ammonia. The Ni_5Co_5/SiO_2-K was evaluated for its stability for 30 h where it showed negligible decrease in conversion and thus excellent stability.

Studies have reported that the stronger basicity of the support the more efficient is the catalyst and thus promoting the catalytic decomposition of ammonia. Therefore, Podila et al. [72] utilized different Mg oxide systems (MgAl, MgCe and MgLa) as supports for cobalt catalysts (5 wt% Co) with Mg to X (X = Al, Ce, La) ratio of 2. Among these three, 5CMLa-2 presented the highest activity. The 5CMAl-2 and the 5CMCe-2 catalysts had lower activities. La-containing catalysts were further studied with different Mg/La molar ratios (Mg/La = 1, 2,3,5,9

and 14). All the catalysts were active even at lower temperatures with 5CMLa-5 being the most active. The higher activity of the 5CMLa-5 catalyst might be due to the increased surface area, higher metal dispersion and the presence of basic sites that favour the ammonia decomposition. It was concluded that Mg-La is a promising support for the reaction of ammonia decomposition.

Pinzón et al. [73] developed Co catalysts supported on β-SiC for the H_2 production by ammonia decomposition at reaction temperatures below 500 ºC. The catalysts were modified with different metals (K, Cs, Ca, Mg, La and Ce) to study the effect of promoters. The catalysts with the addition of 1 % of Cs, Mg, Ca or Ce showed poorer performance while the catalysts loaded with K or La enhanced the catalytic activity due their electron-donor properties that modified the electronic structure of Coactive sites. A conversion of 97.3 % and H_2 production rate of 69.3 mmol H_2 g_{Co}^{-1} min^{-1} was obtained by the 1K-Co/SiC catalyst (4.1 wt % Co) at 450 ºC. Different K loadings were also studied, and results showed that the increase of metal loading above 1% decreased the conversion of ammonia because the excess amount of metal blocked the active sites of the cobalt catalysts. Lastly, the stability of the catalyst was tested for over 24 h at 400 ºC and 83 % conversion of ammonia was reached providing excellent stability.

Table 1. Heterogeneous catalysts used for the ammonia decomposition.

Catalyst	Temperature (ºC)	Conversion (%)	TOF (1/s)	Reference
$Ni/MgAl_2O_4$ – LDH	600	88.7	2.18	[58]
Co/NC-600	500	80		[59]
Ru/SmCeOx	400	74.9	25.81	[60]
35Co/BHA	500	87.2		[61]
2.5Ru/10C-rGO	400	96	75.4	[62]
$CoRe_{1.6}$	500	~90		[63]
K^+-Fe/C	470	20	~0.5	[64]
Ru/Al_2O_3	580		6.85	[65]
Ni/Al_2O_3	580		4.21	[65]
Co-containing CNTs	700	~100		[66]
Fe-containing CNTs	700	76		[66]
(SA-600A)/$RuCl_3.nH_2O$/$LiOH{\cdot}H_2O$ (40:5:3)	490	99.9		[67]
α-FeO_2O_3-50@pSiO_2	800	100		[68]
10%Co/MWCNTs	600		8.15	[69]
$Ru/La_0.33Ce_{0.67}$	450	91.9	11.4	[70]
Ni_5Co_5/SiO_2	550	76.8		[71]
5CMLa-5	550	82.7		[72]
1%K-Co/SiC	350	33.1	9.3	[73]
1%K-Co/SiC	450	97.3		[73]

As observed from Table 1, the temperature ranges from 400 to 800 ^{o}C because ammonia requires higher temperatures for its effective decomposition. At higher temperatures the conversion is higher and in some cases the catalysts achieve almost complete conversion. Even though Ru is a precious and expensive metal, many studies have focused on Ru catalysts due to their excellent catalytic properties [60], [62], [65], [67], [70] . However, other novel catalysts are investigated with promising results for future experiments [58], [61], [63], [66], [73]. Supporting materials are also studied because of their properties for enhanced catalytic operation as they can offer higher surface area, chemical stability and mechanical strength [74]. Generally, the most common ones are alumina and silica [65], [71], but other materials are used as well [59–62], [69], [73].

4.1.1 Structural and physicochemical properties of heterogeneous catalysts

It's necessary to consider any chemical and physical transformation that will occur during the development process of efficient catalysts. The structure and properties of the catalysts play a significant role for the decomposition of any reaction. It is well known that the catalytic decomposition of ammonia is structure sensitive and strongly depends on the size, shape and properties of the catalyst. Mazzone et al. [75] synthesised unpromoted and sodium promoted Ru particles supported on carbon xerogels. The purpose of this study was to investigate the behaviour of the catalysts with support and with or without the promoter. During the second reaction run the un-promoted catalysts exhibited higher reaction rates compared with the first reaction run. The authors explained that the higher reaction rates are due to the formation of B5 sites after the catalyst was exposed at 600 ^{o}C. The B5 sites work in favour of the decomposition reaction, speeding up the N desorption. Sodium as a promoter had a positive effect on the performance of the catalyst preventing the sintering of the Ru particles since the catalyst before and after five runs had the same average particle size for all tested catalysts. In contrast, the un-promoted catalysts presented a slight increase in the mean particle size, e.g., from 1.9 nm to 2.5 nm due to the sintering of Ru particles from high temperatures. The support was either activated with carbon dioxide or doped with nitrogen and both treatments had a positive impact on the catalytic performance.

The effect of particle size was examined by El-Shafie et al. [76] using two different diameters of alumina particles size (1 and 2 mm) for the decomposition of ammonia assisted by dielectric discharge plasma (DBD). The conversion rates and H_2 concentration were measured at different

ammonia flow rates and plasma voltage. Conversion rates of 83.2 and 80.4 % were obtained by Al_2O_3 particle sizes of 1 and 2 mm respectively. Moreover, particle size of 1 mm resulted in higher H_2 concentration. The higher conversion and H_2 concentration are attributed to the higher surface area in the smaller particle and thus, longer residence time for the decomposition reaction. Therefore, it was concluded that the particle size is a significant factor for this catalytic decomposition.

Cobalt catalysts in the form of cobalt oxide (II III) promoted with calcium, aluminium and potassium oxides were developed with precipitation method by Czekajło et al. [77]. With the increase in the precipitation process temperature, it was observed that the size of Co_3O_4 crystallites was reduced leading to a decrease of the efficiency process. The ZBAP1-C catalyst that was promoted with calcium, potassium, and aluminium oxides obtained the highest catalytic activity with a decomposition degree of 100 % at 525 ^oC. The addition of alumina had a positive effect on a shift of the maximum conversion of ammonia towards lower reaction temperatures. The ZBAP1-B catalyst had the lowest surface area value impregnated only with oxides of calcium and potassium while the ZBAP1-C catalyst showed higher resistance in sintering indicating that the addition of aluminium has a positive impact on the stability of the surface structure as well.

Fly ash (FA), a waste material, was used as support for Ru catalysts for H_2 production by ammonia decomposition by Li et al. [78]. The FA samples were acid treated and heat treated, and results showed that treatment enhanced the surface area and pore volume. Ru impregnation further increased the surface area and pore volume on the heat treated and untreated FA samples but decreased on the acid treated samples. From the catalysts used, Ru/FA-800 had the highest conversion of ammonia due to high Ru dispersion, less acid sites and stronger NH_3 adsorption.

Lendzion-Bielun et al. [79] examined the effect of different promoters (CaO, Al_2O_3 and, K_2O) and also the addition of manganese and chromium on the structure of cobalt catalysts for ammonia decomposition. Sintering of pure cobalt was noticed at a temperature of 600 ^oC, but with the addition of the oxides as promoters the surface area of the catalysts was stabilized. The catalytic tests showed that the unpromoted Co catalyst has the lowest activity due to a very low surface area. The Co(0) catalyst that was promoted with the oxides (2.6 wt % Al_2O_3, 1.5 wt % CaO, 0.5 wt % K_2O and 95.4 wt % Co) presented the highest activity at temperatures of 500 and 550 ^oC with NH_3 conversion up to 40.1 and 50 % respectively. Even though an addition

of chromium and manganese lead to an enhancement on the surface area of the catalyst, the activity was decreased.

To investigate the influence of particle size, Li et al. [80] developed Ni particles supported on MCF-17 with particle range size from 1.5 to 8.0 nm. The ammonia decomposition reaction was affected by the particle size of the catalysts especially with small Ni particles. Moreover, the particle size effect was studied at various temperatures and a volcano relationship between the particle size and the catalytic activity was obtained (Fig. 3) proving that the catalysts are structural sensitive. The Ni/MCF-17 catalyst with an average of 3.0 nm particle size exhibited excellent catalytic performance at all temperatures.

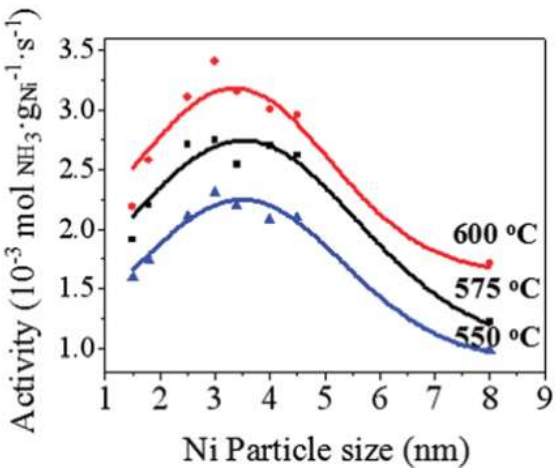

Fig. 3. Effect of the particle size at different reaction temperatures [80].

Besides the correlation between the particle size of catalysts and the catalytic activity, the structure/morphology of the support is important to be explored. Huang et al. [81] studied cobalt catalysts supported on three kinds of CeO_2 supports, 3D ordered mesoporous (3DOM), nanotubes (NT) and nanocubes (NC). The Co/CeO_2-3DOM catalyst exhibited the best catalytic performance with 4.2 mmol H_2 min^{-1} g_{cat} H_2 production rate at 500 °C. According to different characterization techniques that were used in the experiment it was concluded that the particle size was not the main factor to influence the reaction but the different morphologies of the support. The morphology of the Co/CeO_2-3DOM catalyst was favourable for construction of more active sites and thus the better catalytic performance.

4.2 Photocatalysis and Electrocatalysis of Ammonia

Photocatalytic decomposition is considered a promising system for the H_2 production because it can be operated at ambient temperature conditions, and the reaction can be easily controlled

by switching on and off the light irradiation [82–85]. TiO_2 photocatalysts were developed by Abdul Razak et al. [86] that were impregnated with Pd and Cu respectively for enhancement of the photocatalytic activity. After 3 h of light irradiation Pd/TiO_2 exhibited the highest activity producing 65 μmol of H_2 while Cu/TiO_2 and TiO_2 showed almost no production of H_2. For the investigation of the stability of the photocatalysts in alkaline conditions, different NH_3 concentrations were investigated. With a concentration up to 19.1 g/L yield was enhanced up to 30.4 μmol but further increase of NH_3 resulted in a decline of the H_2 production rate. Dimethyl sulfoxide (DMSO) was also added as hydroxyl scavenger in ammonia further enhancing the H_2 yield to 121 μmol and was continuously increasing in the first cycle reaction. However, the rate of H_2 production was reduced with the subsequent reaction cycles and during the photocatalytic decomposition with DMSO methane gas was detected.

Apart from catalysis and photocatalysis, electrochemical decomposition of ammonia has a high potential for supply of CO_x-free energy. Fig. 4 demonstrates a typical ammonia electrolytic cell for hydrogen generation. The most active catalyst for this reaction is Pt and thus lots of research was carried out with Pt catalysts. However, it is very expensive so recent studies are focused on Pt-free catalysts [87–89]. Binary alloy electrocatalysts based on Ni such as Ni-Co, Ni-Mo, Ni-Fe, and Ni-Ce deposited on nickel foam were synthesized by Jiang et al. [90] for the electrochemical generation of H_2 by ammonia. From all the electrodes investigated, Ni-Co in the form of nanoneedle resulted in an impressive electrochemical performance. For further improvement the Ni-Co catalyst was introduced to nitrogen doping and ammonia annealing treatment to obtain $NiCo_2N$ electrodes. The activity was dramatically increased demonstrating a superior HER electrocatalytic performance. The $NiCo_2N$ electrocatalysts also showed an excellent stability as there was no significant change after 10 h of catalytic process. Moreover, it was concluded that the electrolysis potential in ammonia (0.71 V) was much lower than the water splitting suggesting that ammonia electrolysis can replace water electrolysis for H_2 production. Table 2 summarises the results from photocatalysis and electrocatalysis of ammonia.

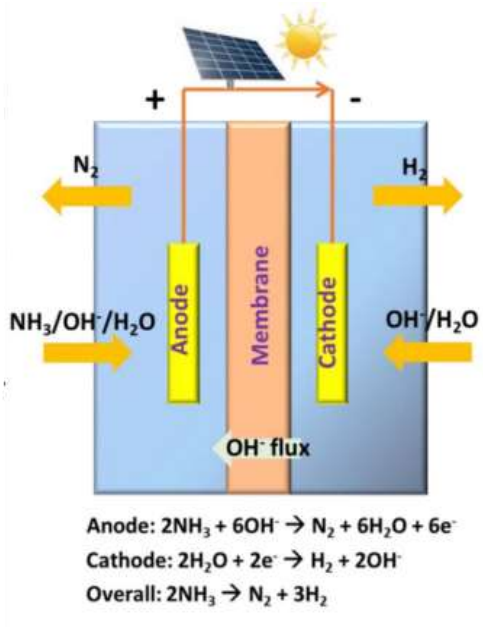

Fig. 4. A typical cell of ammonia electrolysis for hydrogen production [89].

Table 2. Photocatalysts and Electrocatalysts used for ammonia decomposition.

Photocatalysis				
Catalyst	H_2 Yield (μmol)			Reference
Pt/TiO_2	160			[82]
$Pt/Fe\text{-}TiO_2$				[83]
Ce/TiO_2	80			[84]
Pd/TiO_2	65			[86]
Pd/TiO_2-DMSO	121			[86]
Electrocatalysis				
Catalyst	System	Onset Potential	Current Density (mA cm^{-2})	Reference
NiCu/C	55mM NH_4Cl + 0.5 NaOH	0.47 V vs Ag/AgCl	52	[87]
$Ni_{98}Pd_2$	1M $NaNO_3$ + 200mM NH_4NO_3 + NaOH	1.25 V vs Hg/HgO	~2	[88]
$NiCo_2N$	1M KOH + 1M $NH_3.H_2O$	$100x10^{-3}$ V vs RHE	100	[90]

5 Hydrous Hydrazine Decomposition as a sustainable hydrogen production method

5.1 Heterogeneous Catalysis of Hydrous Hydrazine Decomposition

In recent years, the development of efficient catalysts for the decomposition of hydrous hydrazine for H_2 generation has been the focus of many studies. Ni particles were found to be a preferable choice and its alloying with noble metals such as Ir, Pt, Pd and Rh result in a noteworthy improvement on the H_2 selectivity and the catalytic performance due to the alloy synergistic effect [91–93]. Unfortunately, their applications are limited due to the high cost of noble metals. Therefore, it is essential to develop non noble metal containing catalysts. Until now, many studies have reported the decomposition of hydrous hydrazine with noble-metal-free catalysts. Different types of catalysts that were used for the decomposition of hydrous hydrazine are displayed in Table 3.

Noble-metal-free Ni-Fe particles supported on $CeZrO_2$ were synthesised by Zoo et al. [94]. The Ni-Fe/$CeZrO_2$ alloy catalyst with Ni/Fe molar ratio of 8:2 (9.11 wt % Ni and 2.41 wt % Fe) had a TOF value of 119.2 h^{-1} and 100% H_2 selectivity in the presence of NaOH and temperature of 343 K. The catalyst exhibited high stability showing negligible decrease on the H_2 selectivity after five runs. The mean particle size of the Ni-Fe/$CeZrO_2$ catalyst was 5.2 ± 0.8 nm while after five runs was 5.3 ± 1.2 nm. Other supports as $LaZrO_2$ and $NdZrO_2$ also presented excellent catalytic properties. Ni-Co, Ni-Cu and Co-Fe supported on $CeZrO_2$ were also examined and exhibited lower selectivity towards H_2 concluding that NiFe is a highly efficient candidate for the replacement of noble metal catalysts for the hydrous hydrazine decomposition.

Liu et al. [95] synthesized Ni-Mo particles supported on TiO_2 for the catalytic decomposition of hydrous hydrazine. The $Ni_{0.16}Mo_{0.04}/TiO_2$ catalyst with 22.6 wt % Ni and 9.23 wt % Mo exhibited a TOF value of 484 h^{-1} and 100 % H_2 selectivity. Further increase of the support content decreased the catalytic performance, After, 10 cycles the selectivity remained 100% but the TOF decreased to 138 h^{-1}. Ni-Cu/TiO_2, Ni-Fe/ TiO_2, and Ni-Co/TiO_2 catalysts were also prepared for investigation of doping other metals and results showed that the catalytic performances of these catalysts were inferior to Ni-Mo/TiO_2 concluding that Mo doping

improves the dispersion and modifies the geometric and electronic structure of the catalyst facilitating the N_2H_4 decomposition.

Mono-, bi- and tri-metallic noble and noble-metal free catalysts were prepared by Al-Thubaiti et al. [96] to investigate their catalytic activity in the dehydrogenation of hydrous hydrazine. Monometallic Ag, Ni, Pd, Fe and Cu particles were inactive while the activity of bimetallic catalysts was higher. The most active catalyst was the trimetallic Ni/Fe/Pd catalyst that contained 28.7 wt % Ni, 23.5 wt % Fe and 47.7 wt % Pd and average size of 20 nm. It exhibited excellent selectivity towards H_2 and therefore was used for further experiments. After five continuous runs the catalytic activity of the catalyst remained the same. It was concluded by the authors that adding a third metal in a bimetallic catalyst with a specific combination has a positive impact on the selectivity of H_2. Fig. 5 shows the proposed mechanism for the decomposition of ammonia on the surface of the Ni/Fe/Pd catalyst. Moreover, new catalysts can be developed with different metal plating order for the decomposition of hydrazine for H_2 production.

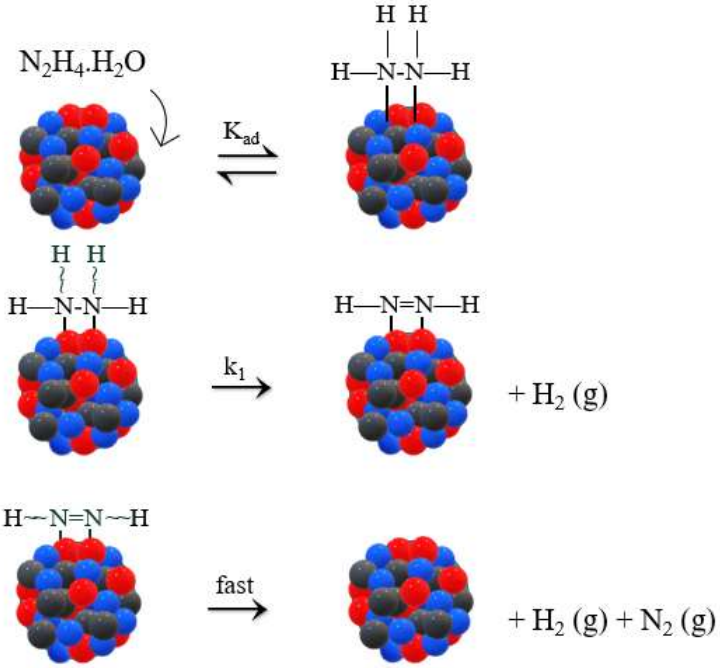

Fig. 5. Decomposition mechanism of hydrous hydrazine on the surface of the trimetallic Ni/Fe/Pd catalyst [96].

Different elements (Rh, Co, Ru, Ir, Cy, Ni, Fe, Pt, Pd NPs) were studied as catalysts for the decomposition of hydrous hydrazine for H_2 production by Sanjay et al. [97]. It was found that the catalytic activity and the selectivity were depended on the catalyst used. Rh was the most

active catalyst whereas Cu, Ni, Fe, Pt and Pd were inactive for the reaction in aqueous solution even though they were active in the reaction that took place in the gas-phase. In the case of Co, Ru and Ir the selectivity towards H_2 was very low. The reason this is happening is because Co, Ru and Ir nanoparticles prefer the activation of the N-N bond which is formatting ammonia. In comparison Rh particles prefer the activation of N-H bond and that's why they are highly active. Moreover, it was observed that the catalytic activity was enhanced when the Rh particles were reduced with $NaBH_4$ in the presence of hexadecyltrimethyl ammonium bromide concluding that the modification of nanoparticles during their preparation could affect their efficiency.

Motta et al. [98] investigated the catalytic performance of Ir/CeO_2 as catalyst for the decomposition of hydrous hydrazine to generate H_2. Parameters such as stirring speed, mass of catalyst, NaOH concentration and reaction temperature were studied to find the optimal conditions for the reaction with respect on the activity and selectivity of the catalytic decomposition. Stirring rate affected both the reaction rate and the selectivity and it was found that with lower stirring rate the H_2 yield was also lower. The optimum stirring rate was 1050 rpm and was used for the following tests. The mass of the catalyst did not affect the yield of the reaction but there was an increase in the activity for molar ratios between 125:1 and 250:1 and the latter were selected for the further catalytic tests. With an increase of the NaOH concentration there was an increase in H_2 yield and 0.5 M NaOH was chosen as the optimal value. Lastly, with an increase in the temperature the selectivity decreased in contrast with the activity of the catalyst that was increased so the value of 50 ^{o}C was chosen because of the intermediate values of activity and selectivity that exhibited. The fresh catalyst had a mean particle size of 0.9 ± 0.2 nm and after five uses 1.2 ± 0.4 nm where the difference was in the range of the error analysis.

Kang et al. [99] developed Ni/CeO_2 catalysts for the decomposition of hydrous hydrazine. A solution combustion synthesis (SCS) varying different parameters was used to synthesize the catalysts and catalytic tests were run under 50 ^{o}C. It was obtained that catalysts with smaller Ni size particle and larger pore size act in favour of the decomposition resulting in a good catalytic performance. 6 wt % Ni/CeO_2 catalysts with 14.7 nm mean particle size and 18.8 nm pore size, exhibited a H_2 selectivity of 100 %, $N_2H_4.H_2O$ conversion of 50 % at 17.7 min corresponding to a TOF value of 34.0 h^{-1}. Moreover, the formation of Ni-O-Ce solid promoted the reaction for H_2 generation, but higher concentrations decreased the catalytic activity. A 30-

608 fold increase of the reaction rate was obtained when increasing the temperature from 30 to 90
609 ^{o}C but the selectivity dropped at 93 %. Lastly, for comparison purposes, Ni-based catalysts
610 developed with different methods were tested and even though a high number of parameters
611 need to be considered, it was concluded that the catalysts created by the SCS method had better
612 catalytic performance.

613 An alloy of Ni-Pd nanoparticles ($Ni_{1-x}Pd_x$) were synthesized by Singh et al. [100] and were
614 examined under mild reaction conditions. The $Ni_{0.60}Pd_{0.40}$ catalyst exhibited the highest
615 selectivity (82 %) among the others tested. To test the effect of alloy, a physical mixture of Ni
616 and Pd was tested and performed poor catalytic activity compared with the alloy catalyst
617 indicating that the modified catalyst surface favours this reaction. The combination of Pd with
618 other metals (Fe, Co and Cu) resulted poor catalytic performance (or inactive) as well as
619 implying that the presence of Ni has a positive effect on the decomposition of hydrous
620 hydrazine.

621 He et al. [101] developed Ni-based catalysts by using Ni-Al hydrotalcite-like compound as
622 precursors. A conversion of 100 % was exhibited with a H_2 selectivity of 93 % at 30 ^{o}C and 70
623 min reaction time. The high selectivity can be attributed to the small Ni particles and strong
624 basic sites. When the temperature increased up to 80 ^{o}C, the reaction time decreased at 5 min
625 and the selectivity was reduced to 82 %. A Ni/Al_2O_3-IMP catalyst was also tested for the
626 decomposition of hydrous hydrazine and compared with Ni-Al_2O_3-HT. A lower activity was
627 noticed by the Ni/Al_2O_3-IMP catalyst with H_2 selectivity at 66 % and 440 min of reaction time
628 due to the poor Ni dispersion.

629 Amorphous catalytic Co-Pt particles induced on CeO_x were developed by Song-Il et al. [102].
630 It was discovered that the CeOx plays a crucial role in the transformation of the crystalline
631 phase to the amorphous one. The highest catalytic performance among the catalysts tested was
632 achieved by the $Co_{0.65}Pt_{0.30}(CeOx)_{0.05}$ nanoalloy, at 25 ^{o}C with H_2 selectivity of 72.1 % in 3.5
633 min and TOF value of 194.8 h^{-1} which is even higher than that of the crystalline phase catalyst.
634 Therefore, it was concluded by the authors that $Co_{0.65}Pt_{0.30}(CeOx)_{0.05}$ exhibited the most
635 optimum performance encouraging its practical use for the decomposition of $N_2H_4.H_2O$ to
636 produce H_2.

637 Several studies used Rh-Ni alloy catalysts supported on different materials for the
638 decomposition of hydrous hydrazine. Zhang et al. [103] developed CeO_x-doped Rh-Ni particles
639 supported on reduced graphene oxide (rGO). The $Rh_{0.8}Ni_{0.2}$@CeOx/rGO catalyst completely

decomposed N_2H_4 at room temperature in 33 min with a TOF value of 36.4 h^{-1}. Further increase in the temperature at 60 ^oC, catalysed the reaction in 3.0 min giving a TOF value of 400.0 h^{-1}. Other studies used MOFs for the support of catalytic materials and therefore RhNi@MIL-101 [104] and Ni-Rh/NPC-900 [105] were developed and tested at 50 ^oC and alkaline conditions 0.5 NaOH. High TOF values of 344 h^{-1} and 156 h^{-1} were exhibited respectively with 100 % H_2 selectivity. Other supports that were used in these studies presented inferior catalytic performance.

Dai et al. [106] synthesized bimetallic Ni-Ir alloy nano-catalysts supported on CeO_2 for the decomposition of hydrous hydrazine for H_2 production. The catalyst showed great catalytic activity and high H_2 selectivity. Further increase on the Ir content ($Ni_{91}Ir_9/CeO_2$) resulted in an optimal catalytic performance and was further investigated. The decomposition rate of hydrous hydrazine increased with increasing the reaction temperature. Also, the catalyst was submitted to cyclic usage, and it was found that it retains 100 % H_2 selectivity even after 15 cycles but the catalytic activity was decreasing after cycle.

Nickel particles were prepared by encapsulation in the channel of TNTs (Ni@TNTs) and deposition on the surface of TNTs (Ni/TNTs) by Wang et al. [107]. Ni@TNTs exhibited high catalytic activity than the Ni/TNTs catalyst and nearly 100 % H_2 selectivity at 333 K. The TOF value of this reaction was 96.0 h^{-1}. The encapsulation of Ni particles led to a small particle size of 2.7 nm, large pore size of 10.2 nm and high dispersion (28.2 %) resulting in more active sites. Moreover, after six continuous catalytic runs the catalyst did not have any significant loss in its catalytic activity due to the prevention of nickel particles leaching during the catalysis, since the particle size had a small increase of 3.5 nm. In contrary, Ni particles on Ni/TNTs increased from 2.4 to 8.9 nm indicating that aggregation is occurring without the TNTs constraining the Ni particles.

Rh nanoparticles modified with Molybdenum Oxide (MoOx) were prepared by Yao et al. [108] with different metal compositions for the catalytic decomposition of hydrous hydrazine and hydrazine borane. Various reaction temperatures were studied and at temperature of 323 K and the presence of $Rh_{0.5}(MoOx)_{0.5}$, N_2H_4 was completely decomposed to H_2 and N_2 with 100% H_2 selectivity and TOF value of 750 h^{-1}. The catalyst had an average mean particle size of 3.8 $\pm$ 0.8 and its composition was 10.05 wt % Rh and 8.92 wt % Mo. It was concluded that the increased catalytic performance obtained by the Rh-based catalysts might encourage the utilisation of hydrous hydrazine as H_2 storage material.

672

673 Table 3. Heterogeneous catalysts utilised for the hydrous hydrazine decomposition.

Catalyst	Temperature (°C)	Conversion (%)	TOF (1/s)	Reference
$Ni_{0.8}Fe_{0.2}/CeZrO_2$	70		0.033	[94]
$Ni_{0.16}Mo_{0.04}/TiO_2$	70	~100	0.134	[95]
Ni/Fe/Pd	40		0.007	[96]
Ir/CeO_2	50	~100	~0.028	[98]
6 wt% Ni/CeO_2	50	50	0.009	[99]
$Ni_{0.60}Pd_{0.40}$	50			[100]
$Ni\text{-}Al_2O_3\text{-HT}$	30	100		[101]
$Co_{0.65}Pt_{0.30}(CeOx)_{0.05}$	25		0.054	[102]
$Rh_{0.8}Ni_{0.2}$@CeOx/rGO	60	100	0.111	[103]
RhNi@MIL-101	50		0.095	[104]
NiRh/NPC-900	50	>50	0.043	[105]
$Ni_{91}Ir_9/CeO_2$	50	100		[106]
Ni@TNTs	60	~100	0.026	[107]
$Rh_{0.5}(MoOx)_{0.5}$	50	100	0.208	[108]

674 Comparing with the temperature range of the ammonia decomposition, as seen from Table 3
675 that hydrous hydrazine decomposition is more favored at lower temperatures (30-70 °C). The
676 most studied temperature is 50 °C giving almost total conversion of hydrous hydrazine [98–
677 100], [104–106], [108]. Nickel is a promising catalyst for this decomposition and by alloying
678 it with other elements, many studies give positive results [94], [95], [99], [101], [107].
679 However, noble metals are often used for the alloys, limiting their application [96], [100], [103–
680 106]. Still research needs to be done though, considering the low TOF values.

681 **5.1.1 Structural and physicochemical properties of heterogeneous catalysts**

682 While the majority of studies are focused on the structure of the catalysts there was no in-depth
683 study of the insights of the microstructure transformations during the synthesis of catalysts
684 which are a key point for the catalytic activity for the hydrous hydrazine decomposition.
685 Therefore Qiu et al. [109] synthesised Ni@Ni-Ir/meso-CeO_2 catalysts for the investigation of
686 the catalytic properties that may be affected by the composition of the surface. Ni@Ir/ meso-
687 CeO_2 resulted from the formation of the Ir surface layer on the Ni particles and with calcination
688 treatment the targeted Ni@Ni-Ir/meso-CeO_2 alloy catalyst was synthesized. The post-treated
689 alloy exhibited excellent activity with a reaction rate of 343 h^{-1} and H_2 selectivity (100 % H_2)
690 at 50 °C, in contrast with the as-prepared catalyst that had lower selectivity and catalytic

performance. It was concluded that the calcination treatment had a positive impact since the Ni@Ir alloy enhanced both the selectivity and catalytic activity.

Shi et al. [110] studied in detail the formation mechanism of the bimetallic $Ni_{50}Pt_{50}/CeO_2$ alloy for the investigation of the influence of preparation process to the structure of the catalyst and thus, the impact on catalytic activity. It was discovered that during the synthesis process the formation of $[(CH_3)_4N]_2PtCl_6$ took place during the co-precipitation step. While increasing the aging time crystalline $[(CH_3)_4N]_2PtCl_6$ disappeared due to the conversion to metallic Pt which was found to have a major impact on the composition and microstructure of the catalyst. As a result, the catalytic performance of the $Ni_{50}Pt_{50}/CeO_2$ catalyst was different depending on the aging time. After 5-12 h of aging time the reaction rate was 465-500 h^{-1} at 30 ^oC which was 2.5 times higher than the reaction time of the catalysts with aging time of 0-1 h.

In another study by Shi et al. [111], noble metal free Ni-W-O alloy nano-catalysts ($Ni_4W/WO_2/NiWO_4$) were synthesised with a hydrothermal process and different reduction temperatures to investigate any changes in the microstructure of the catalysts. Results showed that increasing the annealing treatment temperature the catalytic properties are increased as well. The reduction at 350 ^oC showed both low selectivity and reaction rate while at 400 ^oC selectivity was 99 % and the reaction rate up to 33 h^{-1} with a complete decomposition of hydrazine at 50 ^oC and reaction time of 18 min. Further increase of the annealing treatment temperature reduced the efficiency of the catalyst. Moreover, different characterization analyses were used to better understand if the increased catalytic properties were correlated with the temperature treatment. A decrease on the specific surface area was obtained with the increased reduction temperature that led to the enhanced catalytic performance.

A Ni-Pt/La_2O_3 catalyst was synthesised by Zhong et al. [112] combining alloying and immobilization strategies. The targeted Ni@Ni-Pt/La_2O_3 contained a Ni core and Ni-Pt alloy shell and exhibited 100 % H_2 selectivity. A key factor to achieve great catalytic performance is the formation of the bimetallic alloy therefore the study was not only focused on the catalytic activity of the particles but also the physicochemical surface composition and structure. The excellent catalytic properties were correlated with the electronic and geometric structures changes during the Ni-Pt formation. Moreover, the catalysts were subjected into a second time replacement and calcination treatment under 350 ^oC, and it was observed that both activity and selectivity towards H_2 were increased. It was found that not proper control of the calcination temperature can drastically reduce the performance of the catalyst. In general, there was a

remarkable improvement after the treatment but still the reason behind the enhancement and the dependence of the treatment needs to be further studied.

5.1.2 NH_3 Formation

As it was mentioned hydrous hydrazine can be decomposed by two pathways resulting in the undesirable ammonia production. Thus is a necessity to develop effective catalyst with high selectivity towards H_2. Ni catalysts alloyed with noble metals were a preferred choice by many researchers due to their remarkable enhancement of catalytic properties that resulted from the alloy synergy effect. For example, Singh et al. [93] developed bimetallic Ni-Pt alloy nano-catalysts to enhance the selectivity of Ni nanoparticles that was around 33 % at 323 K. By alloying Ni with Pt content as low as 1 mol % ($Ni_{0.99}Pt_{0.01}$), a complete conversion of $N_2H_4.H_2O$ was obtained in 120 min at 323 K. Further increase of the temperature at 333 K caused a reduction on the reaction time at 70 min with 100 % H_2 selectivity. Authors concluded that the Ni alloying with low Pt content and moderate temperatures are promising for the development of low-cost and high efficiency catalysts for H_2 production by hydrous hydrazine decomposition.

Ni-Ir alloy catalysts supported on Al_2O_3 were investigated by He et al. [113] to compare its activity and selectivity with monometallic Ir/Al_2O_3 and Ni/Al_2O_3 catalysts. $NiIr_{0.016}/Al_2O_3$ (2.0 wt % Ir, 36.8 wt % Ni and 6.1 wt % Al_2O_3) increased the selectivity up to 99 % and the reaction rate was 6.3 h^{-1}. Increasing the Ir molar ratio to Ni up to 0.059, the reaction rate was enhanced at 12.4 h^{-1} and selectivity remained higher than 98%. The stability of the $NiIr_{0.059}/Al_2O_3$ was tested at 10 consecutive cycles at 30 ^oC. The reaction rate decreased to 9.2 h^{-1} but the H_2 selectivity remained over 98%. Reduction of the catalyst at high temperatures resulted in a decreased selectivity and catalytic activity. Moreover, modified Au and Pt Ni/Al_2O_3 catalysts were developed for comparison purposes. $NiPt_{0.027}/Al_2O_3$ exhibited high selectivity while $NiAu_{0.020}/Al_2O_3$ resulted in a lower selectivity and reaction rate as low as 2.0 h^{-1}.

Furthermore, experiments showed that alkaline conditions lead to improved H_2 selectivity. Bimetallic nano-catalysts were developed by alloying Ni and Fe with different Ni/Fe molar ratios by Singh et al. [114] to investigate their catalytic performance for the decomposition of hydrous hydrazine. Even though the catalyst exhibited excellent catalytic activity, the selectivity towards H_2 was only 81 %. With an addition of 0.5 M NaOH the selectivity was enhanced at 100%. The addition of NaOH also improved the selectivity of the $Ni_{45}Pt_{55}$ and

754 $Ni_{50}Ir_{50}$ catalysts from 61 to 86 % and from 7 to 95 % respectively. It was suggested by the
755 authors that the basicity of the NaOH makes the surface of the catalyst basic preventing the
756 formation of NH_3 by the incomplete decomposition of hydrazine and thus promoting the first
757 pathway. Weaker bases such as ammonia and sodium acetate were also examined. Results
758 showed that the addition of these bases had no effect on the catalytic activity and selectivity of
759 the catalysts.

760 Ni particles were synthesised from the reduction of triangular $Ni(HCO_3)_2$ nanosheets and were
761 used as catalysts to produce H_2 by hydrous hydrazine by Wang et al [115]. For the restrain of
762 the NH_3 formation as a side reaction, the effect of NaOH concentration was tested. It was found
763 that with the absence of NaOH the selectivity towards H_2 was 64.5 %. With 0.5M of NaOH,
764 the selectivity was up to 100 % and remained unchanged with further increase of the NaOH
765 concentration. Alkaline conditions speed up the rate determining step of the hydrous hydrazine
766 decomposition and OH^- ions inhibit the formation of ammonia obtaining 100 % H_2 selectivity.

767 Ni-Pt alloy nanoparticles supported on $La_2O_2CO_3$ were developed via an alkali assisted
768 reduction by Yao et al [116]. Among the catalysts tested the $Ni_{0.6}Pt_{0.4}/La_2O_2CO_3$ (2.8 nm)
769 obtained the best catalytic performance with a TOF number of 490 h^{-1} and 100 % H_2 selectivity.
770 After five rounds, the catalyst showed a good stability with only a slight aggregation of 3.4 nm.
771 Further tests were conducted for the evaluation of NaOH effect at the synthesis of the catalysts
772 and during the catalytic process. The catalyst prepared without the addition of NaOH exhibited
773 much lower selectivity and catalytic performance even though NaOH was added during the
774 decomposition reaction. Moreover, the catalyst was synthesised at different NaOH
775 concentrations (0-4 M) and results showed that the efficiency of the catalyst increased until the
776 NaOH concentration was 3 M. These results suggest that NaOH affects both the catalytic
777 process and the preparation of the catalysts. The effect of the NaOH addition at the preparation
778 step of the catalyst and during the process are presented below (Fig. 6).

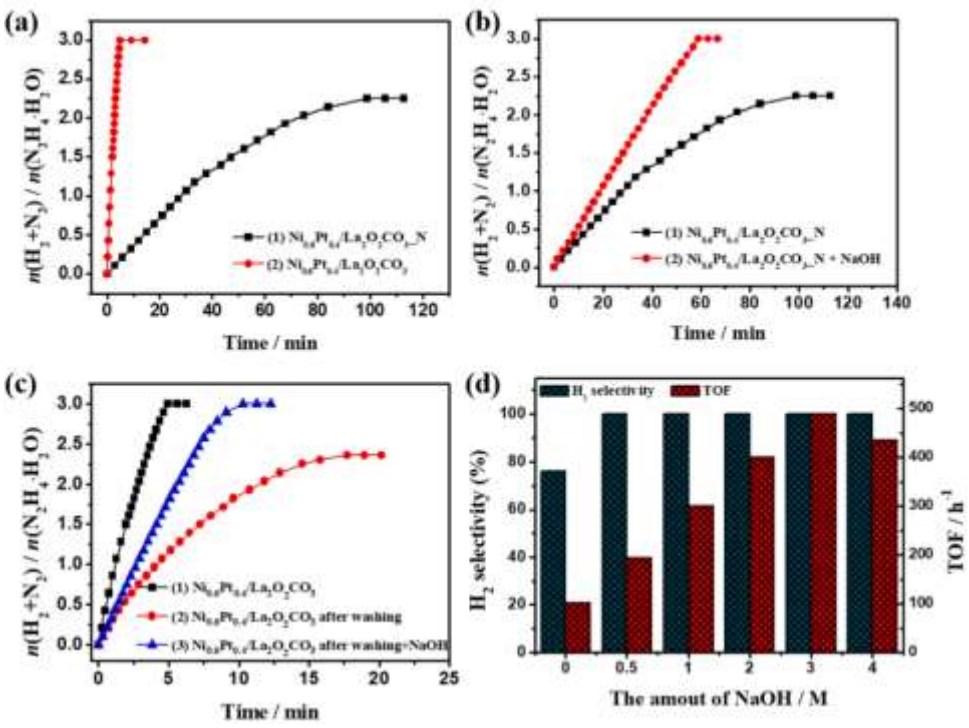

Fig. 6. The effect of NaOH addition in the catalytic decomposition of $N_2H_4.H_2O$ [116].

Huang and Liu [117] examined both the synergistic effect from an Ni alloy and the addition of NaOH to generate H_2 from hydrous hydrazine. Ni-Pt/C catalysts were synthesised with various Pt/Ni molar ratios. The optimal catalytic activity was displayed by Ni_8Pt_1/C and used for further studies with respect to different catalyst concentrations, initial N_2H_4, temperature and NaOH concentration. With an increase on the catalyst concentration and initial N_2H_4 the dehydrogenation rate also increased. The catalytic activity slightly decreased after 5 catalytic runs and characterization results showed that the average grain size of the reused catalyst increased from 2.5 nm to 3.8 nm. At higher temperatures a higher TOF value was obtained. Lastly, with an addition of 0.5 M NaOH, a TOF value of 2640.5 h^{-1} and 100 % H_2 selectivity were obtained at 50 ^oC, while with no addition of the alkaline solution the TOF value was 627.5 h^{-1}.

5.2 Photocatalysis and Electrocatalysis of Hydrous Hydrazine

The catalytic decomposition of hydrous hydrazine for the generation of H_2 is well investigated, but its photocatalytic decomposition still needs lots of research for the discovery of efficient photocatalysts. TiO_2 modified with deposition of noble metals is found to be very promising as for the photocatalytic oxidation of hydrazine and its derivatives [118, 119]. TiO_2

807 nanoparticles modified with rhodium were developed by Kumar et al. [120] for the
808 photocatalytic decomposition of hydrous hydrazine under visible light irradiation. Unmodified
809 TiO_2 particles exhibited a H_2 production of 83 μmol g^{-1} cat and formation rate of 6.9 μmol g^{-1}
810 cat h^{-1} while TiO_2-Rh had a H_2 production of 413 μmol g^{-1} cat and rate formation 42.0 μmol g^{-1}
811 cat h^{-1} after 12 h of visible light irradiation. The photocatalyst was still efficient after five
812 subsequent runs and the H_2 yield was 384 μmol g^{-1} cat but it was noticed a slight decrease in
813 the photoactivity due to leaching of the Rh from the TiO_2 surface. After the five cycles, the
814 value of Rh was 0.14 wt %, slightly lower than that of the fresh catalyst (0.16 wt %).

815 Noble metals such as Pt, Pd and Au were used as electrodes for the electrooxidation of
816 hydrazine to N_2 and H_2 but their high price makes them not practical to use for further
817 applications [121, 122]. Silver nano-catalysts $Ag@C_{60}$ were synthesised by Narwade et al.
818 [123] to investigate the electrocatalytic activity for the oxidation of hydrazine for H_2
819 production. The electrocatalyst was also tested for its efficiency in a range of pH solutions. The
820 best electrochemical performance and long-term stability was exhibited by the $Ag@C_{60}$
821 catalyst in a 0.5 M KOH solution. It was concluded that the enhanced electrocatalytic activity
822 of the $Ag@C_{60}$ is a result of the synergistic effect of Ag nanoparticles and C_{60}.

823 A new method studied recently is the photoelectrocatalysis, a combination of photocatalysis
824 and electrocatalysis. Thus, photoelectrochemical (PEC) H_2 production from $N_2H_4.H_2O$ was
825 studied by Yan et al. [124] using CdS nanorod arrays as the photoelectrode. The proposed
826 mechanism is presented below in Fig. 7. Under visible-light irradiation the photoelectrode in
827 electrolytes with $N_2H_4.H_2O$ presented great stability after 100 h of the reaction while when
828 there were no electrolytes the persistence of the device was less than 100 s. Moreover, the
829 efficiency of the photoelectrode remained the same with a H_2 selectivity over 90 %. The results
830 that were obtained from the CdS photoelectrode promote the PEC H_2 production for further
831 studies and applications. Table 4 summarises the results from the experiments mentioned
832 above.

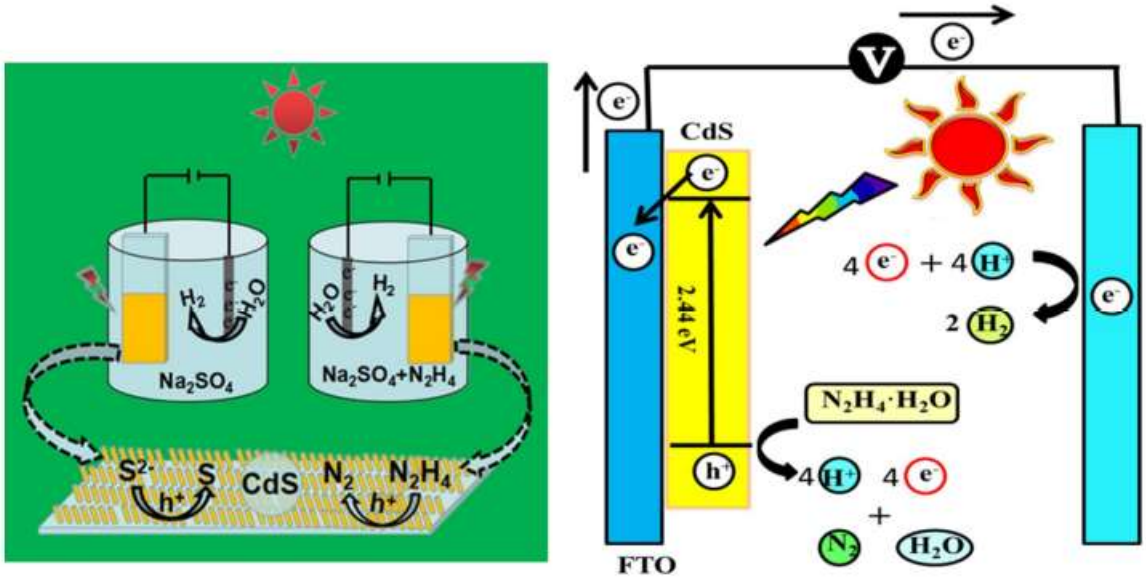

833 Fig. 7. Proposed mechanism of the photoelectrochemical decomposition on CdS nanorod
834 catalysts [124].

835 Table 4. Photocatalysts and Electrocatalysts used for hydrous hydrazine decomposition.

Photocatalysis				
Catalyst	H_2 Yield (μmol)			Reference
Au/TiO_2	48.5			[118]
Pd/SiO_2	1.5			[119]
TiO_2-Rh				[120]
Electrocatalysis				
Catalyst	System	Onset Potential	Current Density (mA cm^{-2})	Reference
$Ni_{60}Co_{40}$	1.0 M KOH + 0.1 M $N_2H_4.H_2O$	1.56 V vs RHE		[121]
Ni/CB	0.1 M NaOH + 0.1 M N_2H_4	0.9245 V vs RHE		[122]
$Ag@C_{60}$	0.5 M KOH + 0.5 mL N_2H_4	0.8 V vs SCE	112	[123]
Photoelectrocatalysis				
CdS NRs	0.1 M Na_2SO_4 + 0.378 M $N_2H_4.H_2O$	1.23 V vs RHE	7.6	[124]

836

6 Reactors for NH_3 decomposition

6.1 Membrane reactors

Catalytic membrane reactors (CMRs) are frequently used for the decomposition of ammonia because they offer several advantages. They shift the thermodynamic equilibrium due to the removal of H_2 allowing the process to proceed at lower temperatures reaching full conversion. Moreover, they do not require an additional separation unit, since separation and purification occur in a single unit, lowering the cost of the system and providing pure H_2. The process is usually assisted by an inert sweep gas that might dilute H_2 stream, which is unwanted. The most suitable materials are Palladium or/and its alloys but their challenging scale-up and high cost limit this technology and therefore new materials must be explored [125].

Numerical simulations for ammonia decomposition in a catalytic membrane reactor filled with Ni/Al_2O_3 catalytic particles were studied by Di Carlo et al [126]. The focus of the study was the evaluation of the improvement of the ammonia decomposition with the use of Pd coated membranes. Firstly, a 2D study was investigated without membranes and results showed that at temperature of 550 ^oC, pressure of 0.2 MPa and low flow velocity of 2cm/s the ammonia conversion was extremely good with a residual NH_3 of only a few ppm. The 3D simulations were studied with the addition of Pd-membranes at 1MPa and temperature range of 500-600 ^oC. At 550 ^oC NH_3 conversion was 99.9% improving almost 18 % the conversion rate that was obtained without the membranes.

A tube-wall catalytic membrane reactor containing a Pd membrane alloyed with Ag ($Pd_{77}Ag_{23}$) was developed by Itoh et al. [127] for the decomposition of ammonia at temperatures below 400 ^oC. A Ru catalyst was used, and the optimal loading was 2 wt % due to the high dispersion on the surface area. A 2 wt % Ru/Al_2O_3 packed bed reactor was compared with the membrane reactor loaded with 2 wt % of Ru and it was found that the latter achieved a higher conversion (about 15% higher) because of the larger heat flux in the tube reactor. The reactor with 2 mm thick Pd membrane achieved 100 % NH_3 conversion at 375 ^oC and ammonia feed rate of 10 mL/min.

Abashar et al. [128] simulated multi-stage Pd-Ag membrane reactors for the generation of ultra-pure H_2. In comparison with a single stage reactor that achieved 29.49 % ammonia conversion the seven-stage membrane reactor exhibited complete conversion of ammonia at 40 bar.

Moreover, a multi-stage fixed bed reactor was modelled under the same conditions and the exit ammonia conversion was 92.37 % suggesting that a multi-stage membrane reactor is superior. The numerical results demonstrated a promising performance of the membrane reactor and even though they were not confirmed experimentally they might have fundamental importance for further design and optimization of the reactor and the process.

Co-based catalysts combined with Pd-Au alloy membranes were demonstrated by Cerrillo et al. [129] for the decomposition of ammonia to the production of high purity H_2. Experiments were carried out with and without the addition of the membrane and results showed that the membrane drastically enhances the conversion of NH_3. The purity of H_2 was > 99.97 % for over 1000 h of running stream. Moreover, the ammonia conversion increased when the temperature, pressure and contact time increased.

Cechetto et al. [130] experimentally demonstrated ammonia decomposition in a catalytic membrane reactor (Fig. 8).The catalyst was Ru-based with double-skin Pd-based membranes. The main focus of the experiments was the purity of H_2 produced in the membrane reactor technology. Results showed that with an increase of the thickness of the membrane above 6 μm ultra-pure H_2 can be generated. Also, a small purification unit can be installed as a more economic feasible solution in contrast with the increase of the membrane thickness. More specifically, a bed of 13X zeolite was tested and it was concluded that it's a suitable sorbent for H_2 purification.

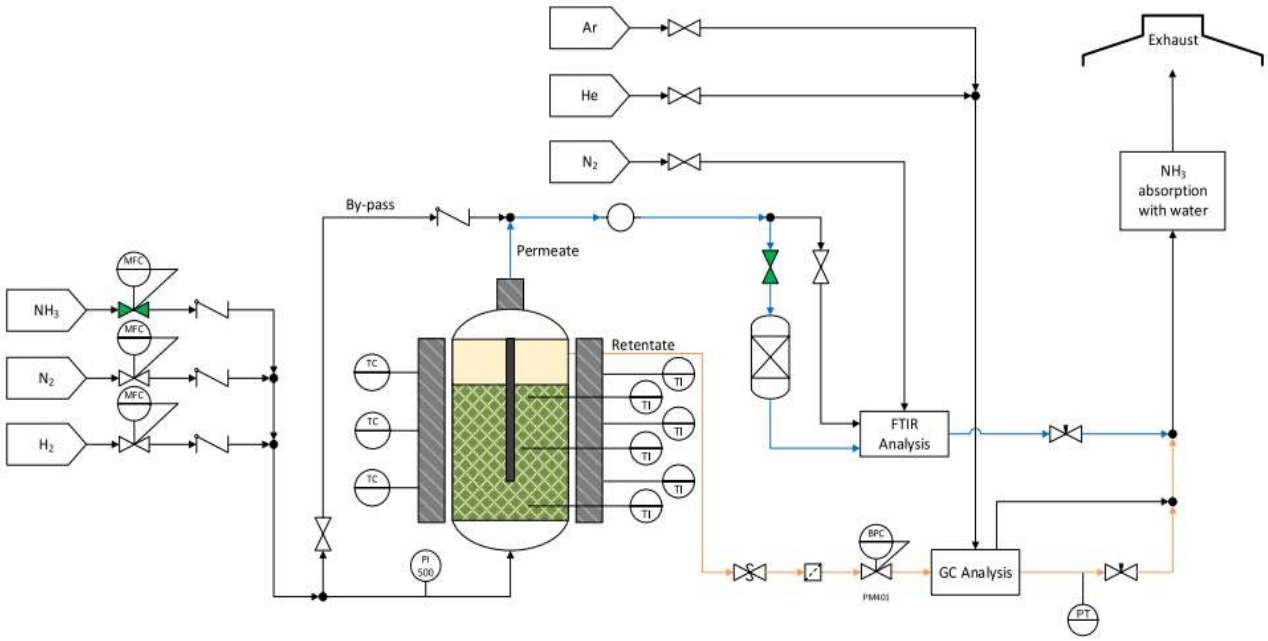

Fig. 8. Process flow diagram of the experimental setup [130].

In addition to that, membranes are required to be free of defects to achieve high H_2 purity. Alternative materials to Pd that have been already used are Vanadium, and Ni alloys. A 3D CFD model was developed by Shwe Hla and Dolan [131] for the examination of the performance of a Vanadium-based alloy membrane reactor for H_2 generation and separation by ammonia decomposition. At 30 L/min NH_3 inlet flow rate, pressure of 7.8 bar_a and 300 ^oC, a conversion of 90 % NH_3 was achieved and H_2 yield over 95 % within a shorter distance along membrane tubes. As expected, at lower inlet flow rates, H_2 yield was higher due to a longer residence time. The effects of the membrane permeability on the H_2 yield were tested under different percentages of the original value. At only 50 % functionality the H_2 yield was similar with that obtained at 100 % membrane permeability.

A double layered $Nd_{5.5}Mo_{0.5}W_{0.5}O_{11.25-\delta}$ (NMW)/ $Nd_{5.5}Mo_{0.5}W_{0.5}O_{11.25-\delta}$-Ni (NMW-Ni) membrane was synthesised by Cheng et al. [132] for the on-site H_2 production by catalytic ammonia decomposition. NMW-NiO layer served as the catalytic reaction site while the NMW layer provided the separation of H_2. A sweep gas of N_2 was used and NH_3 conversion of 99 % was obtained at 750 ^oC, 24% higher than that of a packed bed reactor that was achieved under the same conditions, given to the simultaneous removal of the H_2. Moreover, the highest conversion may be attributed to the longer length of the membrane reactor. It was noticed that NH_3 conversion was higher at lower NH_3 flow rates in the feed stream due to a higher residence time of ammonia in the reactor, whereas H_2 production was small due to a slower composition rate, indicating the need to improve ammonia decomposition at high feed flow rates. After 75 h of reaction at 750 ^oC, the membrane reactor maintained a high conversion of 91 % achieving high long-term stability.

Ru particles dispersed on yttria-stabilized zirconium (YSZ) coated by a Pd film, were developed by Zhang et al. [133] to utilize them for H_2 production by the decomposition of NH_3. The reaction took place in a catalytic membrane reactor. Different parameters such as temperature, pressure and inlet flow were tested to evaluate the reactor performance. An addition of Cs promoter caused complete decomposition of NH_3 at temperatures of 400 ^oC and volumetric H_2 productivity of 31.6 mol m^{-3} s^{-1}. Both the catalyst and the membrane were found to eliminate any transport resistances resulting in a decreased operation temperature, reduced catalyst content and higher H_2 productivity in contrast with a PBMR. Also, a reactor model was developed to better understand the performance of the reactor. The experimental results

were in a great agreement with the model at all conditions, validating the first-order kinetics and the efficiency of the CMR.

6.2 Fixed Bed Reactors

Fixed bed reactors (FBRs) have many large-scale applications in the industry. One great advantage is that the catalyst is immobilized, and the reactant mixture is technically forced to be in contact with it. Though, due to its poor mixing properties large temperature gradients occur and therefore, the extent of the ammonia decomposition can be reduced [134].

Commercial 5 wt% Ru/C catalyst on different promoter Cs loadings was studied experimentally by Chen et al. [135] in a fixed bed reactor for the decomposition of ammonia. The experimental setup that was used in this work is demonstrated in Fig. 9. The optimum Cs/Ru molar ratio was 4.5 and further increase than that resulted in a decrease on the conversion of ammonia. At 400 ^{o}C ammonia conversion was nearly 100 %.

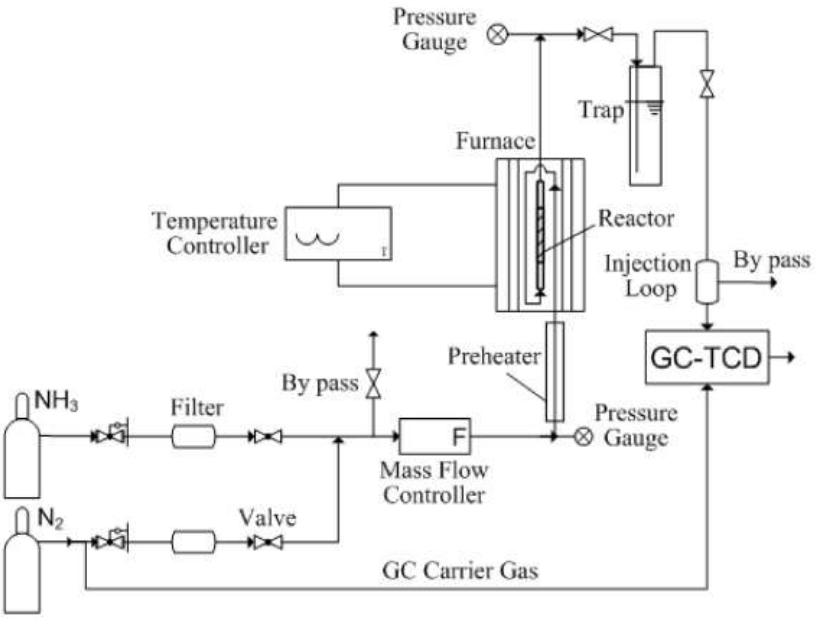

Fig. 9. Schematic diagram of the process for ammonia decomposition in a fixed bed reactor [135].

Gu et al. [136] developed Ni-based catalysts supported in porous alumina (Ni@Al_2O_3) via a simple one-pot method for the decomposition of ammonia. The Ni content was adjusted from 5 at.% to 25 at.% and the reaction took place in a fixed bed reactor. The catalyst with the highest nickel content (25 at. %) exhibited the highest ammonia conversion of 93.9 % at 600 ^{o}C and almost full conversion (99.1 %) at 650 ^{o}C. H_2 formation rate reached up to 7.8 mmol $gcat^{-1}$

947 min^{-1} at 450 ^{o}C. There was an increase in the crystallite size of Ni particles from 1 nm (fresh)
948 to 6 nm (used) due to high reaction temperature. The high catalytic performance could be
949 attributed by the strong interaction amongst the mesoporous alumina matrix and nickel
950 particles that can prevent the metallic Ni from sintering into large aggregates and the high
951 dispersion of Ni particles.

952 A fixed bed plug flow reactor was used by Morlanés et al. [137] for the decomposition of
953 ammonia by Ba-CoCe catalysts with various Co/Ce molar ratios. When catalysts were prepared
954 by impregnation it was noticed that above 20 % of Co loading decreased the conversion of
955 ammonia, while when they were prepared via coprecipitation the opposite trend was found
956 since 30 % Co content catalysts showed higher activity. The high activity could be attributed
957 to the coprecipitation method that allowed higher amounts of Co incorporated in the catalyst.
958 The optimum performance was from the 0.5Ba/CoCe(80/20) catalyst with 41.4 wt % Co, 23.5
959 wt % Ce and 0.45 wt % Ba, whose catalytic activity was comparable with Ru-based catalysts.
960 At 450 ^{o}C it exhibited a conversion little bit lower than 80 %. Ce as a promoter, increased Co
961 dispersion and prevented sintering and aggregation.

962 Ru nanoparticles were supported on alkali silicates (Ru/A_2SiO_3, A = Li, Na and K) by Zhiqiang
963 et al. [138] The catalytic reaction occurred in a fixed bed reactor at atmospheric pressure.
964 Ru/K_2SiO_3 (3.21 wt % Ru) showed the best catalytic performance with an NH_3 conversion of
965 60.5 %, H_2 formation rate of 20.3 mmol $g_{cat}^{-1}min^{-1}$ and TOF value of 2.03 s^{-1} at 450 ^{o}C. A series
966 of K- promoted catalysts were prepared to evaluate the effect of the K content but results
967 showed that the highest ammonia conversion was the one already exhibited by Ru/K_2SiO_3. In
968 comparison with other works that used Ru particles supported on other silicon materials at the
969 same conditions, Ru/K_2SiO_3 achieved higher performance due to a better promotion effect of
970 the alkali metal silicates. It was concluded by the authors that the formation of oxygen
971 vacancies on the alkali metal silicates can stabilize the Ru nanoparticles with strong metal
972 support interactions that results in an increase of the number of active sites.

973 Ni-Ru/CeO_2 catalysts with several metal loadings were prepared by Lucentini et al. [139] and
974 tested for the H_2 generation from the decomposition of ammonia. The catalytic tests were
975 carried in a fixed bed reactor and results showed that the best catalytic performance was
976 observed by 0.4-0.6 wt% Ru and 2.4-5.0 wt % Ni. After 100 h of continuous operation the
977 catalysts exhibited excellent long-term stability. At 400 ^{o}C, TOF values exceeding 2 s^{-1} were
978 obtained. With the use of Langmuir-Hinshelwood-Hougen-Watson approach, a kinetic model

was developed for the simulation of the H_2 production rate under different parameters. Lastly, it was concluded that the limiting step for the reaction is the dehydrogenation of ammonia adsorbed on the surface of the catalysts.

In addition to the previous research Lucentini et al. [140] continued the investigation on the decomposition of ammonia on Ni-Ru catalysts supported on 3D-printed CeO_2 structures in a fixed bed reactor. The $Ni_{0.5}Ru_{0.1}$ catalyst achieved the best catalytic performance and therefore was used for the rest of the study. Moreover, a 1D mathematical model was developed over the 3D-printed catalytic structure loaded with Ni-Ru catalysts. A comparison between the experimental results and the simulation validated the model that was developed. For the optimisation of the catalytic structure, a series of simulations were performed with different geometric parameters to examine their effect on the catalytic performance in ammonia decomposition. Specifically, the geometric parameters that were optimized were the wall thickness, the number and width of channels for better and more efficient usage of the reactor with the intention of on-site generation H_2 and usage in a PEM-type fuel cell.

Co_3Mo_3N and γ-Mo_2N catalysts were synthesised with the use of citric acid as a chelating agent by Jolaoso et al. [141]. The catalytic tests were performed in a fixed bed quartz tube reactor at atmospheric pressure, a temperature range of 300-600 ^oC and constant GHSV of 6000 h^{-1}. At 550 ^oC, γ-Mo_2N catalyst gave 71.9 % NH_3 conversion while Co_3Mo_3N gave 97.3 % resulting in a better catalytic performance indicating that Co particles promote the ammonia decomposition. Characterization tests showed that Co_3Mo_3N catalyst contained 33.72 wt %, 54.41 wt % and 4.03 wt % Co, Mo and N respectively. After 35 h of a continuous test the catalyst showed no deactivation. This was validated by measuring the crystallite size of the fresh catalyst (6.20 nm) and the used catalyst (6.19 nm) whereas no significant decrease was obtained. Conversion of 100 % was obtained by both catalysts at 600 ^oC.

Another study conducted in a fixed bed reactor, implemented three Ru-supported catalysts (Ru/Al_2O_3, Ru/La_2O_3-Al_2O_3 and $Ru/La_2O_2CO_3$-Al_2O_3). Kim et al. [142] examined their catalytic activity at a low temperature range of 350-500^oC. The best catalytic activity was established by $Ru/La_2O_2CO_3$-Al_2O_3 (11.5 wt % La and 0.95 wt % Ru) with 80.1 % NH_3 conversion at 500 ^oC. Even though characterization tests showed that Ru/Al_2O_3 had higher Ru dispersion (27.3 %) than Ru/La_2O_3-Al_2O_3 (20.6 %) it resulted in a lower catalytic activity suggesting that the La addition promoted electron donation from La to Ru particles due to their electronegativity difference and therefore increasing the kinetics of the reaction. Moreover, the

La oxycarbonate-rich surface favoured the formation of Ru particles on the surface of the catalyst preventing the particles to leave from the surface into the bulk phase. Thus, it was concluded that the $La_2O_2CO_3$ surface coating might be beneficial for catalyst synthesis when an increased surface metal concentration is needed.

6.3 Microreactors

Microreactors gained attention in the early 1990s marking them as a relatively new field. Microreactor technology offers better control, high surface area ratios, high heat and mass transfer rates and enhanced conversion efficiency. Compared with conventional reactors, micro structured reactors exhibited higher activity towards NH_3 ammonia decomposition [143].

An autothermal microchannel reactor was evaluated for the decomposition of ammonia to generate H_2 and provide it for power generation systems. Engelbrecht, Chiuta and Bessarabov [144] studied the effects of different parameters such as NH_3 decomposition flow rate and oxidation flow rate and fuel-oxygen equivalence ratio to find the optimal operation parameters. The catalyst for decomposition was 8.5 wt % Ru/Al_2O_3 and for the oxidation was 5 wt % Pt/Al_2O_3. A conversion up to 99.8% was observed with a H_2 equivalent fuel power of 0.71 kWe, when the decomposition flow rate was 6 NL mim-1, the oxidation flow rate was 4 NL min^{-1} and the fuel-oxygen ratio was 1.4. A stability test was also carried out for 24 h in demanding reactor conditions to determine any inconsistencies in the catalyst where results showed that no deactivation of the catalyst occurred during reaction. It was concluded that the performance of the reactor was good and further research might be able to up-scale this system for multi-kW power generation systems.

Based on the experimental results obtained from Engelbrecht, Chiuta and Bessarabov [144], a 3D CFD model was developed by Schumacher et al. [145] to study both steady-state and transient regimes in a microchannel reactor to provide a suitable mathematical model. In consideration of the wide range of ammonia decomposition and oxidation flow rates and temperature profiles, the simulation fitted the experimental data with an acceptable accuracy. It was found that at the microreactor inlet the highest temperature was obtained and therefore a different solution needed to be developed to solve the model with regard in the distribution of heat transfer. Therefore, any future reactor designs should be focused on the optimization of the heat transfer rate.

3D printed SiCN monolithic ceramic microreactors and Ru catalysts were used by Gyak et al. [146] for ammonia decomposition at high temperature. A temperature range of 500-1000 ^{o}C and different flow rates of 2, 4 and 8 mL min^{-1} were the conditions for the catalytic reaction. At 2 mL min^{-1} and 1000 ^{o}C, ammonia was completely decomposed due to an increased residence time. After 48 h of exposure to ammonia and 1000 ^{o}C, the ceramic microreactors demonstrated excellent chemical resistance and heat tolerance.

Maleki, Fulton and Bertola [147] designed a microreactor, both experimentally and numerically for H_2 production via low temperature ammonia decomposition over $Co_{0.5}Ce_{0.1}Al_{0.4}O$(sa) catalyst. The geometries of the microchannel are presented in Fig. 10. Two kinetic models were used to describe the reaction, a pseudo-first order model and a modified Temkin-Pyzhev model that were compiled in a CFD model. The model then was solved at a various NH_3 flow rates and temperatures and exhibited good agreement with the experimental data. At a lower temperature range the Temkin-Pyzhev model had better accuracy than the first model and therefore was selected for further study. Higher conversion rates were obtained while increasing the temperatures whereas over 99 % was observed at temperatures of 550 ^{o}C.

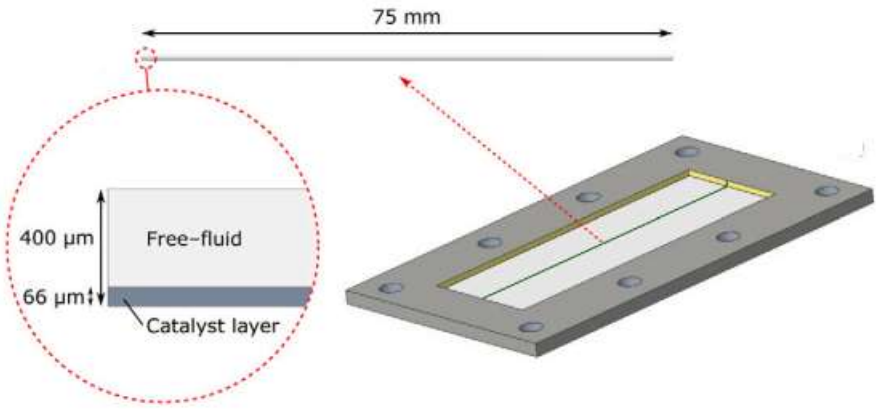

Fig. 10. 2D and 3D geometries of the microreactor [147].

Bimetallic Ru-Fe alloy catalysts were synthesised and impregnated with carbon nanotubes by Chen et al. [148] The experiments took place in a fixed bed microreactor at a temperature range of 300-500 ^{o}C and atmospheric pressure. The Ru_3Fe/CNTs catalyst (1.67 wt % Ru, 0.31 wt % Fe) presented the best catalytic performance in contrast with the Ru/CNTs catalyst. At 500 ^{o}C both catalysts resulted in a 100 % ammonia conversion. After 60 h of reaction, the activity of Ru/CNTs was decreased by 30 % while that of Ru_3Fe/CNTs decreased only 10 % exhibiting superior stability with the addition of Ru. It was concluded that the alloy synergistic effect

between Ru and Fe enhanced the catalytic activity and furthermore the addition of the non-noble metal Fe reduces the content of Ru resulting in a lower catalyst cost.

Table 5. A summary of the type of reactors used for ammonia decomposition.

Type of reactor	Catalyst	Temperature	Conversion	Yield	TOF	Reference
Pd membrane reactor	Ni/Al_2O_3	550	99.9			[126]
Pd membrane reactor	$2\%Ru/Al_2O_3$	375	100			[127]
Pd-Ag membrane reactor			100			[128]
Pd-Au membrane reactor	Co			99.97		[129]
Double-skin Pd membrane reactor	Ru			93.2		[130]
Vanadium alloy membrane reactor		300	90	>95		[131]
NMW/NMW-NiO	NMW-NiO powder	750	99			[132]
YSZ/Pd membrane reactor	Ru	400	93	90		[133]
Fixed bed reactor	5%Ru/C	400	~100			[135]
Fixed bed reactor	$25\%Ni@Al_2O_3$	650	99.1			[136]
Fixed bed reactor	0.5Ba/CoCe(80/20)	450	74		0.602	[137]
Fixed bed reactor	Ru/K_2SiO_3	450	60.5		2.03	[138]
Fixed bed reactor	$Ni\text{-}Ru/CeO_2$	400			2	[139]
Fixed bed reactor	$Ni\text{-}Ru/CeO_2$					[140]
Fixed bed reactor	Co_3Mo_3N	550	97.3			[141]
Fixed bed reactor	$Ru/La_2O_2CO_3\text{-}Al_2O_3$	500	80.1			[142]
Microreactor	$8.5\%Ru/Al_2O_3$	651	99.8			[144]
Microreactor – Experimental	Ru/Al_2O_3	300	99.9			[145]
Microreactor – Simulation	Ru/Al_2O_3	300	99.9			[145]
Microreactor	Ru	1000	100			[146]
Microreactor	$Co_{0.5}Ce_{0.1}Al_{0.4}O(sa)$	550	99			[147]
Microreactor	$Ru_3Fe/CNTs$	500	100		86.21	[148]

As seen from Table 5 membrane reactors and microreactors are superior to fixed bed reactors. Even though membrane reactors are well studied, the most common membrane used is Pd and its alloys [126–130], [133], which is rare and expensive and needs to be replaced with other elements that give off such high catalytic activity and selectivity. Regarding fixed bed reactors, a number of studies give promising results but most of them presented low conversion of ammonia [137–139], [142]. The need for high temperatures for the decomposition makes these reactors unsuitable. Studies on microreactors operating experimentally and theoretically in a

large range of temperatures are limited mostly for Ru-based catalysts as they present high catalytic activity giving the opportunity for further development of a cost-effective reactor system [145, 146], [148].

7 Conclusions

Green energy carriers have the potential to solve the current issues related with climate change. An emerging energy resource is H_2 as an alternative to non-renewable sources such as conventional fuels. Its physical storage though, is limiting its application. Therefore, this review provides information about ammonia and hydrous hydrazine as possible chemical hydrogen storage compounds. Moreover, heterogeneous catalysts utilized for the decomposition reactions of the compounds mentioned above are reviewed in contrast with their efficiency. An issue occurring with hydrous hydrazine decomposition is ammonia formation that can lead to corrosion and lower selectivity regarding H_2. The most promising catalytic system for ammonia decomposition is ruthenium and its alloys but it's not methodical due to its high price and scarcity. For hydrous hydrazine, the most active catalytic system is nickel catalysts alloyed with noble metals that are some of the most expensive metals in the world. Thus, there is a great need for the development of cost-effective catalytic systems for both ammonia and hydrous hydrazine, using more abundant metals instead of precious metals with lower metal loading and higher atom efficiency. Reactor technology used for NH_3 decomposition has also been presented in this review. The most common catalyst used for this reaction is the catalytic membrane reactor. Due to the membrane, separation and purification can occur in a single step, giving pure H_2 and lowering the operation cost. Palladium membranes were found to be the most suitable materials, but future works need to take into consideration their high cost and therefore, explore and develop other materials with the same efficacy. Microreactors are also an attractive option due to a high activity towards NH_3 with different types of catalysts, especially ruthenium and its alloys. In contrast, fixed bed reactors presented lower activity and further research is needed for future applications and up-scaled production of H_2. In conclusion, for on-site hydrogen production by NH_3 and $N_2H_4.H_2O$ future research must give attention to the development of low-cost catalyst with optimum catalytic performance and great selectivity towards H_2. Furthermore, it's important to consider the reactor technology and develop systems with low operation cost and high efficiency.

References

[1] K. Mazloomi and C. Gomes, “Hydrogen as an energy carrier: Prospects and challenges,” *Renew. Sustain. Energy Rev.*, vol. 16, no. 5, pp. 3024–3033, Jun. 2012, doi: 10.1016/J.RSER.2012.02.028.

[2] A. Pareek, R. Dom, J. Gupta, J. Chandran, V. Adepu, and P. H. Borse, “Insights into renewable hydrogen energy: Recent advances and prospects,” *Mater. Sci. Energy Technol.*, vol. 3, pp. 319–327, Jan. 2020, doi: 10.1016/J.MSET.2019.12.002.

[3] S. Shiva Kumar and V. Himabindu, “Hydrogen production by PEM water electrolysis – A review,” *Mater. Sci. Energy Technol.*, vol. 2, no. 3, pp. 442–454, Dec. 2019, doi: 10.1016/J.MSET.2019.03.002.

[4] S. Atilhan, S. Park, M. M. El-Halwagi, M. Atilhan, M. Moore, and R. B. Nielsen, “Green hydrogen as an alternative fuel for the shipping industry,” *Curr. Opin. Chem. Eng.*, vol. 31, Mar. 2021, doi: 10.1016/J.COCHE.2020.100668.

[5] M. Ji and J. Wang, “Review and comparison of various hydrogen production methods based on costs and life cycle impact assessment indicators,” *Int. J. Hydrogen Energy*, vol. 46, no. 78, pp. 38612–38635, Nov. 2021, doi: 10.1016/J.IJHYDENE.2021.09.142.

[6] K. Scott, “Chapter 1 Introduction to Electrolysis, Electrolysers and Hydrogen Production,” *RSC Energy Environ. Ser.*, vol. 2020-January, no. 25, pp. 1–27, 2019, doi: 10.1039/9781788016049-00001.

[7] R. A. Felseghi, E. Carcadea, M. S. Raboaca, C. N. Trufin, and C. Filote, “Hydrogen Fuel Cell Technology for the Sustainable Future of Stationary Applications,” *Energies 2019, Vol. 12, Page 4593*, vol. 12, no. 23, p. 4593, Dec. 2019, doi: 10.3390/EN12234593.

[8] S. Zhang, Z. He, X. Li, J. Zhang, Q. Zang, and S. Wang, “Building heterogeneous nanostructures for photocatalytic ammonia decomposition,” *Nanoscale Adv.*, vol. 2, no. 9, pp. 3610–3623, 2020, doi: 10.1039/d0na00161a.

[9] Y. Kojima, “Hydrogen storage materials for hydrogen and energy carriers,” *Int. J. Hydrogen Energy*, vol. 44, no. 33, pp. 18179–18192, 2019, doi: 10.1016/j.ijhydene.2019.05.119.

[10] M. Aziz, A. TriWijayanta, and A. B. D. Nandiyanto, “Ammonia as effective hydrogen storage: A review on production, storage and utilization,” *Energies*, vol. 13, no. 12, pp. 1–25, 2020, doi: 10.3390/en13123062.

[11] M. J. Palys and P. Daoutidis, “Using hydrogen and ammonia for renewable energy storage: A geographically comprehensive techno-economic study,” *Comput. Chem. Eng.*, vol. 136, p. 106785, 2020, doi: 10.1016/j.compchemeng.2020.106785.

[12] M. Tawalbeh, S. Z. M. Murtaza, A. Al-Othman, A. H. Alami, K. Singh, and A. G. Olabi, “Ammonia: A versatile candidate for the use in energy storage systems,” *Renew. Energy*, vol. 194, pp. 955–977, 2022, doi: 10.1016/j.renene.2022.06.015.

[13] K. E. Lamb, M. D. Dolan, and D. F. Kennedy, “Ammonia for hydrogen storage; A review of catalytic ammonia decomposition and hydrogen separation and purification,” *Int. J. Hydrogen Energy*, vol. 44, no. 7, pp. 3580–3593, 2019, doi: 10.1016/j.ijhydene.2018.12.024.

[14] W. Ramsay and S. Young, “The decomposition of ammonia by heat,” no. 88, pp. 88–93, 1884.

[15] E. P. Perman and G. A. S. Atkinson, “The decomposition of ammonia by heat,” vol. 44, pp. 110–117, 1904.

[16] B. Robert Matt air, H. H. Sisler, F. Raschig, and V. Chemie GmbH, “Hydrazine from Chlorine with Anhydrous Ammonia The Production of Hydrazine by the Reaction of Chlorine with Anhydrous Ammonia1.”

[17] S. Zhong and Q. Xu, “Metal nanoparticle-catalyzed hydrogen generation from liquid chemical hydrides,” *Bull. Chem. Soc. Jpn.*, vol. 91, no. 11, pp. 1606–1617, 2018, doi: 10.1246/bcsj.20180227.

[18] D. X. Zhang, H. Yin, H. F. Zhong, L. Y. Gan, and P. Wang, “Linear scaling relations for N2H4 decomposition over transition metal catalysts,” *Int. J. Hydrogen Energy*, vol. 45, no. 32, pp. 16114–16121, 2020, doi: 10.1016/j.ijhydene.2020.04.054.

[19] S. Prabu, M. Vinu, and K. Y. Chiang, “Metal nanoparticles supported on crystalline Al(OH)3 Nano sheets for efficient catalytic hydrogen production from hydrous hydrazine in aqueous solution,” *Int. J. Energy Res.*, vol. 45, no. 13, pp. 18857–18874, 2021, doi: 10.1002/er.6975.

[20] V. A. Matyshak and O. N. Silchenkova, “Catalytic Decomposition of Hydrazine and Hydrazine Derivatives to Produce Hydrogen-Containing Gas Mixtures: A Review,” *Kinet. Catal.*, vol. 63, no. 4, pp. 339–350, 2022, doi: 10.1134/s0023158422040073.

[21] L. Zhou, X. Luo, L. Xu, C. Wan, and M. Ye, “Pt-Ni nanoalloys for H2 generation from Hydrous Hydrazine,” *Catalysts*, vol. 10, no. 8, 2020, doi: 10.3390/catal10080930.

[22] R. Tarkowski, “Underground hydrogen storage: Characteristics and prospects,” *Renew. Sustain. Energy Rev.*, vol. 105, no. January, pp. 86–94, 2019, doi: 10.1016/j.rser.2019.01.051.

[23] Alexander Körner, “Technology Roadmap Hydrogen and Fuel Cells,” 2015.

[24] J. Zheng, X. Liu, P. Xu, P. Liu, Y. Zhao, and J. Yang, “Development of high pressure gaseous hydrogen storage technologies,” *Int. J. Hydrogen Energy*, vol. 37, no. 1, pp. 1048–1057, Jan. 2012, doi: 10.1016/J.IJHYDENE.2011.02.125.

[25] E. Rivard, M. Trudeau, and K. Zaghib, “Hydrogen storage for mobility: A review,” *Materials (Basel).*, vol. 12, no. 12, 2019, doi: 10.3390/ma12121973.

[26] Z. Free, M. Hernandez, M. Mashal, and K. Mondal, “A review on advanced manufacturing for hydrogen storage applications,” *Energies*, vol. 14, no. 24, 2021, doi: 10.3390/en14248513.

[27] D. P. Broom and M. Hirscher, “Irreproducibility in hydrogen storage material research,” *Energy Environ. Sci.*, vol. 9, no. 11, pp. 3368–3380, 2016, doi: 10.1039/c6ee01435f.

[28] A. C. Dillon, K. M. Jones, T. A. Bekkedahl, C. H. Kiang, D. S. Bethune, and M. J. Heben, “Storage of hydrogen in single-walled carbon nanotubes,” *Nature*, vol. 386. pp. 377–379, 1997.

[29] A. Chambers, C. Park, R. Terry, K. Baker, and N. M. Rodriguez, “Hydrogen Storage in Graphite Nanofibers,” vol. 102, 1998.

[30] M. Becher *et al.*, “Hydrogen storage in carbon nanotubes,” *Comptes Rendus Phys.*, vol. 4, no. 9, pp. 1055–1062, 2003, doi: 10.1016/S1631-0705(03)00107-5.

[31] G. G. Tibbetts, G. P. Meisner, and C. H. Olk, “Hydrogen storage capacity of carbon nanotubes, filaments, and vapor-grown fibers,” *Carbon N. Y.*, vol. 39, no. 15, pp. 2291–2301, 2001, doi: 10.1016/S0008-6223(01)00051-3.

[32] M. Rzepka *et al.*, “Hydrogen Storage Capacity of Catalytically Grown Carbon Nanofibers,” 2005, doi: 10.1021/jp051371a.

[33] S. Liu, L. Guo, H. Jin, L. Li, G. Li, and L. Yu, “Hydrogen production by supercritical water gasification of coal: A reaction kinetic model including nitrogen and sulfur elements,” *Int. J. Hydrogen Energy*, vol. 45, no. 56, pp. 31732–31744, Nov. 2020, doi: 10.1016/J.IJHYDENE.2020.08.166.

[34] S. I. Ngo, Y. Il Lim, W. Kim, D. J. Seo, and W. L. Yoon, “Computational fluid dynamics and experimental validation of a compact steam methane reformer for hydrogen production from natural gas,” *Appl. Energy*, vol. 236, pp. 340–353, Feb. 2019, doi: 10.1016/J.APENERGY.2018.11.075.

[35] H. H. Cho, V. Strezov, and T. J. Evans, “Environmental impact assessment of hydrogen production via steam methane reforming based on emissions data,” *Energy Reports*, vol. 8, pp. 13585–13595, Nov. 2022, doi: 10.1016/J.EGYR.2022.10.053.

[36] M. H. Ali Khan, R. Daiyan, P. Neal, N. Haque, I. MacGill, and R. Amal, “A framework for assessing economics of blue hydrogen production from steam methane reforming using carbon capture storage & utilisation,” *Int. J. Hydrogen Energy*, vol. 46, no. 44, pp. 22685–22706, Jun. 2021, doi: 10.1016/J.IJHYDENE.2021.04.104.

[37] M. Yu, K. Wang, and H. Vredenburg, “Insights into low-carbon hydrogen production methods: Green, blue and aqua hydrogen,” *Int. J. Hydrogen Energy*, vol. 46, no. 41, pp. 21261–21273, Jun. 2021, doi: 10.1016/J.IJHYDENE.2021.04.016.

[38] S. Hafeez *et al.*, “Decomposition of Additive-Free Formic Acid Using a Pd/C Catalyst in Flow: Experimental and CFD Modelling Studies,” *Catal. 2021, Vol. 11, Page 341*, vol. 11, no. 3, p. 341, Mar. 2021, doi: 10.3390/CATAL11030341.

[39] S. Hafeez *et al.*, “Experimental and process modelling investigation of the hydrogen generation from formic acid decomposition using a pd/zn catalyst,” *Appl. Sci.*, vol. 11, no. 18, 2021, doi: 10.3390/app11188462.

[40] J. Chi and H. Yu, “Water electrolysis based on renewable energy for hydrogen production,” *Cuihua Xuebao/Chinese J. Catal.*, vol. 39, no. 3, pp. 390–394, Mar. 2018, doi: 10.1016/S1872-2067(17)62949-8.

[41] M. Hermesmann and T. E. Müller, “Green, Turquoise, Blue, or Grey? Environmentally

friendly Hydrogen Production in Transforming Energy Systems," *Prog. Energy Combust. Sci.*, vol. 90, May 2022, doi: 10.1016/J.PECS.2022.100996.

[42] F. Dawood, M. Anda, and G. M. Shafiullah, "Hydrogen production for energy: An overview," *Int. J. Hydrogen Energy*, vol. 45, no. 7, pp. 3847–3869, Feb. 2020, doi: 10.1016/J.IJHYDENE.2019.12.059.

[43] A. E. Karaca, I. Dincer, and J. Gu, "Life cycle assessment study on nuclear based sustainable hydrogen production options," *Int. J. Hydrogen Energy*, vol. 45, no. 41, pp. 22148–22159, Aug. 2020, doi: 10.1016/J.IJHYDENE.2020.06.030.

[44] S. E. Hosseini and M. A. Wahid, "Hydrogen from solar energy, a clean energy carrier from a sustainable source of energy," *Int. J. Energy Res.*, vol. 44, no. 6, pp. 4110–4131, 2020, doi: 10.1002/er.4930.

[45] A. Boretti, "There are hydrogen production pathways with better than green hydrogen economic and environmental costs," *Int. J. Hydrogen Energy*, vol. 46, no. 46, pp. 23988–23995, Jul. 2021, doi: 10.1016/J.IJHYDENE.2021.04.182.

[46] M. Noussan, P. P. Raimondi, R. Scita, and M. Hafner, "The role of green and blue hydrogen in the energy transition—a technological and geopolitical perspective," *Sustain.*, vol. 13, no. 1, pp. 1–26, 2021, doi: 10.3390/su13010298.

[47] G. Baskar, R. Aiswarya, S. Soumiya, N. Mohanapriya, and S. Roselin Nivetha, "Recent Advances in Heterogeneous Catalysts for Biodiesel Production," *J. Energy Environ. Sustain.*, vol. 4, pp. 1–5, Jul. 2017, doi: 10.47469/JEES.2017.V04.100038.

[48] D. J. Richardson, K. Hellgardt, P. A. Russell, G. Mason, and B. A. Buffman, "Flux Response Analysis: A Study of Ammonia Decomposition Over Pt/Alumina," *Chem. Eng. Res. Des.*, vol. 82, no. 10, pp. 1397–1403, Oct. 2004, doi: 10.1205/CERD.82.10.1397.46741.

[49] J. Polanski *et al.*, "Ni-Supported Pd Nanoparticles with Ca Promoter: A New Catalyst for Low-Temperature Ammonia Cracking," *PLoS One*, vol. 10, no. 8, p. e0136805, Aug. 2015, doi: 10.1371/JOURNAL.PONE.0136805.

[50] C. Huang *et al.*, "Ru/La 2 O 3 catalyst for ammonia decomposition to hydrogen," *Appl. Surf. Sci.*, vol. 476, no. November 2018, pp. 928–936, 2019, doi: 10.1016/j.apsusc.2019.01.112.

[51] C. Popa, W. K. Offermans, R. A. Van Santen, and A. P. J. Jansen, “Ab initio density-functional theory study of NH x dehydrogenation and reverse reactions on the Rh(111) surface,” doi: 10.1103/PhysRevB.74.155428.

[52] S. Mukherjee, S. V. Devaguptapu, A. Sviripa, C. R. F. Lund, and G. Wu, “Low-temperature ammonia decomposition catalysts for hydrogen generation,” *Appl. Catal. B Environ.*, vol. 226, no. August 2017, pp. 162–181, 2018, doi: 10.1016/j.apcatb.2017.12.039.

[53] S. F. Yin, B. Q. Xu, X. P. Zhou, and C. T. Au, “A mini-review on ammonia decomposition catalysts for on-site generation of hydrogen for fuel cell applications,” *Appl. Catal. A Gen.*, vol. 277, no. 1–2, pp. 1–9, 2004, doi: 10.1016/j.apcata.2004.09.020.

[54] B. Lorenzut *et al.*, “Embedded Ru@ZrO 2 Catalysts for H2 Production by Ammonia Decomposition,” vol. 2, no. 9, pp. 1096–1106, 2010, doi: 10.1002/cctc.201000097.

[55] A. Takahashi and T. Fujitani, “Kinetic Analysis of Decomposition of Ammonia over Nickel and Ruthenium Catalysts,” *J. Chem. Eng. Japan*, vol. 49, no. 1, pp. 22–28, 2016, doi: 10.1252/jcej.14we431.

[56] X. Ju *et al.*, “Mesoporous Ru/MgO prepared by a deposition-precipitation method as highly active catalyst for producing COx-free hydrogen from ammonia decomposition,” *Appl. Catal. B Environ.*, vol. 211, pp. 167–175, 2017, doi: 10.1016/j.apcatb.2017.04.043.

[57] C. Chen *et al.*, “Ru-Based Catalysts for Ammonia Decomposition: A Mini-Review,” *Energy and Fuels*, vol. 35, no. 15, pp. 11693–11706, 2021, doi: 10.1021/acs.energyfuels.1c01261.

[58] Y. Qiu, E. Fu, F. Gong, and R. Xiao, “Catalyst support effect on ammonia decomposition over Ni/MgAl2O4 towards hydrogen production,” *Int. J. Hydrogen Energy*, vol. 47, no. 8, pp. 5044–5052, 2022, doi: 10.1016/j.ijhydene.2021.11.117.

[59] G. Li, H. Zhang, X. Yu, Z. Lei, F. Yin, and X. He, “Highly efficient Co/NC catalyst derived from ZIF-67 for hydrogen generation through ammonia decomposition,” *Int. J. Hydrogen Energy*, vol. 47, no. 26, pp. 12882–12892, 2022, doi: 10.1016/j.ijhydene.2022.02.046.

[60] H. Tang *et al.*, “Catalytic activity of Ru supported on SmCeOx for ammonia decomposition: The effect of Sm doping,” *J. Solid State Chem.*, vol. 295, no. October 2020, p. 121946, 2021, doi: 10.1016/j.jssc.2020.121946.

[61] G. Li, X. Yu, F. Yin, Z. Lei, H. Zhang, and X. He, “Production of hydrogen by ammonia decomposition over supported Co3O4 catalysts,” *Catal. Today*, vol. 402, no. November 2021, pp. 45–51, 2022, doi: 10.1016/j.cattod.2022.02.020.

[62] M. Pinzón, O. Avilés-García, A. R. de la Osa, A. de Lucas-Consuegra, P. Sánchez, and A. Romero, “New catalysts based on reduced graphene oxide for hydrogen production from ammonia decomposition,” *Sustain. Chem. Pharm.*, vol. 25, no. January, 2022, doi: 10.1016/j.scp.2022.100615.

[63] K. G. Kirste *et al.*, “COx-free hydrogen production from ammonia – mimicking the activity of Ru catalysts with unsupported Co-Re alloys,” *Appl. Catal. B Environ.*, vol. 280, no. August 2020, p. 119405, 2021, doi: 10.1016/j.apcatb.2020.119405.

[64] A. Jedynak, Z. Kowalczyk, D. Szmigiel, W. Raróg, and J. Zieliński, “Ammonia decomposition over the carbon-based iron catalyst promoted with potassium,” *Appl. Catal. A Gen.*, vol. 237, no. 1–2, pp. 223–226, 2002, doi: 10.1016/S0926-860X(02)00330-7.

[65] J. C. Ganley, F. S. Thomas, E. G. Seebauer, and R. I. Masel, “A priori catalytic activity correlations: The difficult case of hydrogen production from ammonia,” *Catal. Letters*, vol. 96, no. 3–4, pp. 117–122, 2004, doi: 10.1023/B:CATL.0000030108.50691.d4.

[66] J. Zhang, M. Comotti, F. Schüth, R. Schlögl, and D. S. Su, “Commercial Fe- or Co-containing carbon nanotubes as catalysts for NH 3 decomposition,” *Chem. Commun.*, no. 19, pp. 1916–1918, 2007, doi: 10.1039/b700969k.

[67] M. El-Shafie, S. Kambara, and Y. Hayakawa, “Development of zeolite-based catalyst for enhancement hydrogen production from ammonia decomposition,” *Catal. Today*, vol. 397–399, no. March 2021, pp. 103–112, 2022, doi: 10.1016/j.cattod.2021.11.022.

[68] M. Feyen *et al.*, “High-temperature stable, iron-based core-shell catalysts for ammonia decomposition,” *Chem. - A Eur. J.*, vol. 17, no. 2, pp. 598–605, 2011, doi: 10.1002/chem.201001827.

[69] H. Zhang *et al.*, “Tuning catalytic performances of cobalt catalysts for clean hydrogen

generation via variation of the type of carbon support and catalyst post-treatment temperature," *Int. J. Hydrogen Energy*, vol. 39, no. 31, pp. 17573–17582, 2014, doi: 10.1016/j.ijhydene.2014.07.183.

[70] T. A. Le *et al.*, "Ru-supported lanthania-ceria composite as an efficient catalyst for COx-free H2 production from ammonia decomposition," *Appl. Catal. B Environ.*, vol. 285, no. September 2020, p. 119831, 2021, doi: 10.1016/j.apcatb.2020.119831.

[71] Z. W. Wu, X. Li, Y. H. Qin, L. Deng, C. W. Wang, and X. Jiang, "Ammonia decomposition over SiO2-supported Ni–Co bimetallic catalyst for COx-free hydrogen generation," *Int. J. Hydrogen Energy*, vol. 45, no. 30, pp. 15263–15269, 2020, doi: 10.1016/j.ijhydene.2020.04.007.

[72] S. Podila, Y. A. Alhamed, A. A. Alzahrani, and L. A. Petrov, "Hydrogen production by ammonia decomposition using Co catalyst supported on Mg mixed oxide systems," *Int. J. Hydrogen Energy*, vol. 40, no. 45, pp. 15411–15422, 2015, doi: 10.1016/j.ijhydene.2015.09.057.

[73] M. Pinzón, A. Romero, A. de Lucas-Consuegra, A. R. de la Osa, and P. Sánchez, "COx-free hydrogen production from ammonia at low temperature using Co/SiC catalyst: Effect of promoter," *Catal. Today*, vol. 390–391, no. November 2021, pp. 34–47, 2022, doi: 10.1016/j.cattod.2021.12.005.

[74] Y. Sakata, Y. Tamaura, H. Imamura, and M. Watanabe, "Preparation of a new type of CaSiO3 with high surface area and property as a catalyst support," *Stud. Surf. Sci. Catal.*, vol. 162, pp. 331–338, 2006, doi: 10.1016/S0167-2991(06)80924-9.

[75] S. Mazzone, T. Goklany, G. Zhang, J. Tan, E. I. Papaioannou, and F. R. García-García, "Ruthenium-based catalysts supported on carbon xerogels for hydrogen production via ammonia decomposition," *Appl. Catal. A Gen.*, vol. 632, no. January, p. 118484, 2022, doi: 10.1016/j.apcata.2022.118484.

[76] M. El-Shafie, S. Kambara, and Y. Hayakawa, "Alumina particle size effect on H2 production from ammonia decomposition by DBD plasma," *Energy Reports*, vol. 6, pp. 25–30, 2020, doi: 10.1016/j.egyr.2020.10.032.

[77] Ł. Czekajło and Z. Lendzion-Bieluń, "Effect of preparation conditions and promoters on the structure and activity of the ammonia decomposition reaction catalyst based on

nanocrystalline cobalt," *Chem. Eng. J.*, vol. 289, pp. 254–260, 2016, doi: 10.1016/j.cej.2015.12.093.

[78] L. Li, S. Wang, Z. Zhu, X. Yao, and Z. Yan, "Catalytic decomposition of ammonia over fly ash supported Ru catalysts," *Fuel Process. Technol.*, vol. 89, no. 11, pp. 1106–1112, 2008, doi: 10.1016/j.fuproc.2008.05.002.

[79] Z. Lendzion-Bielun, U. Narkiewicz, and W. Arabczyk, "Cobalt-based catalysts for ammonia decomposition," *Materials (Basel).*, vol. 6, no. 6, pp. 2400–2409, 2013, doi: 10.3390/ma6062400.

[80] Y. Li *et al.*, "Size structure-catalytic performance correlation of supported Ni/MCF-17 catalysts for CO: X-free hydrogen production," *Chem. Commun.*, vol. 54, no. 49, pp. 6364–6367, 2018, doi: 10.1039/c8cc01884g.

[81] C. Huang *et al.*, "Hydrogen generation by ammonia decomposition over Co/CeO2 catalyst: Influence of support morphologies," *Appl. Surf. Sci.*, vol. 532, no. July, 2020, doi: 10.1016/j.apsusc.2020.147335.

[82] H. Kominami, H. Nishimune, Y. Ohta, Y. Arakawa, and T. Inaba, "Photocatalytic hydrogen formation from ammonia and methyl amine in an aqueous suspension of metal-loaded titanium(IV) oxide particles," *Appl. Catal. B Environ.*, vol. 111–112, pp. 297–302, 2012, doi: 10.1016/j.apcatb.2011.10.011.

[83] K. Obata, K. Kishishita, A. Okemoto, K. Taniya, Y. Ichihashi, and S. Nishiyama, "Photocatalytic decomposition of NH3 over TiO2 catalysts doped with Fe," *Appl. Catal. B Environ.*, vol. 160–161, no. 1, pp. 200–203, 2014, doi: 10.1016/j.apcatb.2014.05.033.

[84] M. Reli *et al.*, "Novel cerium doped titania catalysts for photocatalytic decomposition of ammonia," *Appl. Catal. B Environ.*, vol. 178, pp. 108–116, 2015, doi: 10.1016/j.apcatb.2014.10.021.

[85] A. Iwase, K. Ii, and A. Kudo, "Decomposition of an aqueous ammonia solution as a photon energy conversion reaction using a Ru-loaded ZnS photocatalyst," *Chem. Commun.*, vol. 54, no. 48, pp. 6117–6119, Jun. 2018, doi: 10.1039/C8CC02639D.

[86] S. Abdul Razak, A. H. Mahadi, R. Thotagamuge, D. Prasetyoko, and H. Bahruji, "Photocatalytic Hydrogen Gas Production from NH3 and Alkylamine: Route to Zero

Carbon Emission Energy," *Catal. Letters*, no. 0123456789, 2022, doi: 10.1007/s10562-022-04049-5.

[87] W. Xu *et al.*, "Electrodeposited NiCu bimetal on carbon paper as stable non-noble anode for efficient electrooxidation of ammonia," *Appl. Catal. B Environ.*, vol. 237, pp. 1101–1109, 2018, doi: 10.1016/j.apcatb.2016.11.003.

[88] A. Allagui, S. Sarfraz, S. Ntais, F. Al Momani, and E. A. Baranova, "Electrochemical behavior of ammonia on Ni98Pd2 nano-structured catalyst," *Int. J. Hydrogen Energy*, vol. 39, no. 1, pp. 41–48, 2014, doi: 10.1016/j.ijhydene.2013.10.024.

[89] N. M. Adli, H. Zhang, S. Mukherjee, and G. Wu, "Review—Ammonia Oxidation Electrocatalysis for Hydrogen Generation and Fuel Cells," *J. Electrochem. Soc.*, vol. 165, no. 15, pp. J3130–J3147, 2018, doi: 10.1149/2.0191815jes.

[90] K. Jiang *et al.*, "Nickel-cobalt nitride nanoneedle supported on nickel foam as an efficient electrocatalyst for hydrogen generation from ammonia electrolysis," *Electrochim. Acta*, vol. 403, p. 139700, 2022, doi: 10.1016/j.electacta.2021.139700.

[91] Z. Zhang, S. Zhang, Q. Yao, X. Chen, and Z. H. Lu, "Controlled Synthesis of MOF-Encapsulated NiPt Nanoparticles toward Efficient and Complete Hydrogen Evolution from Hydrazine Borane and Hydrazine," *Inorg. Chem.*, vol. 56, no. 19, pp. 11938–11945, 2017, doi: 10.1021/acs.inorgchem.7b01910.

[92] D. Bhattacharjee, K. Mandal, and S. Dasgupta, "High performance nickel-palladium nanocatalyst for hydrogen generation from alkaline hydrous hydrazine at room temperature," *J. Power Sources*, vol. 287, pp. 96–99, 2015, doi: 10.1016/j.jpowsour.2015.04.008.

[93] S. K. Singh, Z. H. Lu, and Q. Xu, "Temperature-induced enhancement of catalytic performance in selective hydrogen generation from hydrous hydrazine with Ni-based nanocatalysts for chemical hydrogen storage," *Eur. J. Inorg. Chem.*, no. 14, pp. 2232–2237, 2011, doi: 10.1002/ejic.201100083.

[94] H. Zou, Q. Yao, M. Huang, M. Zhu, F. Zhang, and Z. H. Lu, "Noble-metal-free NiFe nanoparticles immobilized on nano CeZrO2 solid solutions for highly efficient hydrogen production from hydrous hydrazine," *Sustain. Energy Fuels*, vol. 3, no. 11, pp. 3071–3077, 2019, doi: 10.1039/c9se00547a.

[95] X. Liu, Y. Liu, J. Wang, and J. Ma, “Anatase-Type TiO2-Modified Amorphous NiMo Nanoparticles with Superior Catalytic Performance toward Dehydrogenation of Hydrous Hydrazine,” *Ind. Eng. Chem. Res.*, vol. 61, no. 4, pp. 1636–1643, 2022, doi: 10.1021/acs.iecr.1c03398.

[96] K. S. Al-Thubaiti and Z. Khan, “Trimetallic nanocatalysts to enhanced hydrogen production from hydrous hydrazine: The role of metal centers,” *Int. J. Hydrogen Energy*, vol. 45, no. 27, pp. 13960–13974, 2020, doi: 10.1016/j.ijhydene.2020.03.093.

[97] S. K. Singh, X. B. Zhang, and Q. Xu, “Room-temperature hydrogen generation from hydrous hydrazine for chemical hydrogen storage,” *J. Am. Chem. Soc.*, vol. 131, no. 29, pp. 9894–9895, 2009, doi: 10.1021/ja903869y.

[98] D. Motta, I. Barlocco, S. Bellomi, A. Villa, and N. Dimitratos, “Hydrous hydrazine decomposition for hydrogen production using of ir/ceo2: Effect of reaction parameters on the activity,” *Nanomaterials*, vol. 11, no. 5, pp. 1–15, 2021, doi: 10.3390/nano11051340.

[99] W. Kang and A. Varma, “Hydrogen generation from hydrous hydrazine over Ni/CeO2 catalysts prepared by solution combustion synthesis,” *Appl. Catal. B Environ.*, vol. 220, no. April 2017, pp. 409–416, 2018, doi: 10.1016/j.apcatb.2017.08.053.

[100] S. K. Singh, Y. Iizuka, and Q. Xu, “Nickel-palladium nanoparticle catalyzed hydrogen generation from hydrous hydrazine for chemical hydrogen storage,” *Int. J. Hydrogen Energy*, vol. 36, no. 18, pp. 11794–11801, 2011, doi: 10.1016/j.ijhydene.2011.06.069.

[101] L. He *et al.*, “A Noble-Metal-Free Catalyst Derived from Ni-Al Hydrotalcite for Hydrogen Generation from N2H4·H2O Decomposition,” *Angew. Chemie*, vol. 124, no. 25, pp. 6295–6298, 2012, doi: 10.1002/ange.201201737.

[102] O. Song-Il, J. M. Yan, H. L. Wang, Z. L. Wang, and Q. Jiang, “High catalytic kinetic performance of amorphous CoPt NPs induced on CeOx for H2 generation from hydrous hydrazine,” *Int. J. Hydrogen Energy*, vol. 39, no. 8, pp. 3755–3761, 2014, doi: 10.1016/j.ijhydene.2013.12.135.

[103] Z. Zhang, Z.-H. Lu, H. Tan, X. Chen, and Q. Yao, “CeO x-modified RhNi nanoparticles grown on rGO as highly efficient catalysts for complete hydrogen generation from hydrazine borane and hydrazine †,” *J. Mater. Chem. A*, vol. 3, pp.

23520–23529, 2015, doi: 10.1039/c5ta06197k.

[104] P. Zhao, N. Cao, W. Luo, and G. Cheng, “Nanoscale MIL-101 supported RhNi nanoparticles: An efficient catalyst for hydrogen generation from hydrous hydrazine,” *J. Mater. Chem. A*, vol. 3, no. 23, pp. 12468–12475, 2015, doi: 10.1039/c5ta02201k.

[105] B. Xia, K. Chen, W. Luo, and G. Cheng, “NiRh nanoparticles supported on nitrogen-doped porous carbon as highly efficient catalysts for dehydrogenation of hydrazine in alkaline solution,” *Nano Res.*, vol. 8, no. 11, pp. 3472–3479, 2015, doi: 10.1007/s12274-015-0845-4.

[106] H. Dai, Y. Zhong, and P. Wang, “Hydrogen generation from decomposition of hydrous hydrazine over Ni-Ir/CeO2 catalyst,” *Prog. Nat. Sci. Mater. Int.*, vol. 27, no. 1, pp. 121–125, 2017, doi: 10.1016/j.pnsc.2016.12.012.

[107] H. Wang *et al.*, “Ni nanoparticles encapsulated in the channel of titanate nanotubes : E ffi cient noble-metal-free catalysts for selective hydrogen generation from hydrous hydrazine,” *Chem. Eng. J.*, vol. 332, no. July 2017, pp. 637–646, 2018, doi: 10.1016/j.cej.2017.09.126.

[108] Q. Yao, M. He, X. Hong, X. Chen, G. Feng, and Z. H. Lu, “Hydrogen production via selective dehydrogenation of hydrazine borane and hydrous hydrazine over MoOx-promoted Rh catalyst,” *Int. J. Hydrogen Energy*, vol. 44, no. 53, pp. 28430–28440, 2019, doi: 10.1016/j.ijhydene.2019.02.105.

[109] Y. P. Qiu, H. Yin, H. Dai, L. Y. Gan, H. Bin Dai, and P. Wang, “Tuning the Surface Composition of Ni/meso-CeO2 with Iridium as an Efficient Catalyst for Hydrogen Generation from Hydrous Hydrazine,” *Chem. - A Eur. J.*, vol. 24, no. 19, pp. 4902–4908, 2018, doi: 10.1002/chem.201705923.

[110] Q. Shi, Y. P. Qiu, H. Dai, and P. Wang, “Study of formation mechanism of Ni-Pt/CeO2 catalyst for hydrogen generation from hydrous hydrazine,” *J. Alloys Compd.*, vol. 787, pp. 1187–1194, 2019, doi: 10.1016/j.jallcom.2019.01.378.

[111] Q. Shi *et al.*, “Noble-Metal-Free Ni-W-O-Derived Catalysts for High-Capacity Hydrogen Production from Hydrazine Monohydrate,” *ACS Sustain. Chem. Eng.*, vol. 8, no. 14, pp. 5595–5603, 2020, doi: 10.1021/acssuschemeng.9b07782.

[112] Y. J. Zhong *et al.*, “Highly efficient Ni@Ni-Pt/La2O3 catalyst for hydrogen generation

from hydrous hydrazine decomposition: Effect of Ni-Pt surface alloying," *J. Power Sources*, vol. 300, pp. 294–300, 2015, doi: 10.1016/j.jpowsour.2015.09.071.

[113] L. He *et al.*, "Structural and catalytic properties of supported Ni-Ir alloy catalysts for H2 generation via hydrous hydrazine decomposition," *Appl. Catal. B Environ.*, vol. 147, pp. 779–788, 2014, doi: 10.1016/j.apcatb.2013.10.022.

[114] S. K. Singh, A. K. Singh, K. Aranishi, and Q. Xu, "Noble-Metal-Free Bimetallic Nanoparticle-Catalyzed Selective," pp. 19638–19641, 2011.

[115] H. Wang, L. Wu, Y. Wang, X. Li, and Y. Wang, "Facile synthesis of Ni nanoparticles from triangular Ni(HCO3)2 nanosheets as catalysts for hydrogen generation from hydrous hydrazine," *Catal. Commun.*, vol. 100, no. March, pp. 33–37, 2017, doi: 10.1016/j.catcom.2017.06.021.

[116] Q. Yao *et al.*, "Alkali-assisted synthesis of ultrafine NiPt nanoparticles immobilized on La2O2CO3 for highly efficient dehydrogenation of hydrous hydrazine and hydrazine borane," *Catal. Today*, vol. 400–401, no. June 2021, pp. 49–58, 2022, doi: 10.1016/j.cattod.2021.11.023.

[117] W. Huang and X. Liu, "The 'on–off' switch for on-demand H2 evolution from hydrous hydrazine over Ni8Pt1/C nano-catalyst," *Fuel*, vol. 315, no. January, p. 123210, 2022, doi: 10.1016/j.fuel.2022.123210.

[118] M. Hinojosa-Reyes, A. Hernández-Gordillo, R. Zanella, and V. Rodríguez-González, "Renewable hydrogen harvest process by hydrazine as scavenging electron donor using gold TiO2 photocatalysts," *Catal. Today*, vol. 266, pp. 2–8, 2016, doi: 10.1016/j.cattod.2015.10.002.

[119] A. E. Raevskaya *et al.*, "Photocatalytic H2 production from aqueous solutions of hydrazine and its derivatives in the presence of nitric-acid-activated graphitic carbon nitride," *Catal. Today*, vol. 284, pp. 229–235, 2017, doi: 10.1016/j.cattod.2016.12.024.

[120] P. Kumar *et al.*, "Visible light assisted hydrogen generation from complete decomposition of hydrous hydrazine using rhodium modified TiO2 photocatalysts," *Photochem. Photobiol. Sci.*, vol. 16, no. 7, pp. 1036–1042, 2017, doi: 10.1039/c6pp00432f.

[121] J. Sanabria-Chinchilla, K. Asazawa, T. Sakamoto, K. Yamada, H. Tanaka, and P.

Strasser, “Noble metal-free hydrazine fuel cell catalysts: EPOC effect in competing chemical and electrochemical reaction pathways,” *J. Am. Chem. Soc.*, vol. 133, no. 14, pp. 5425–5431, 2011, doi: 10.1021/ja111160r.

[122] T. Y. Jeon, M. Watanabe, and K. Miyatake, “Carbon segregation-induced highly metallic Ni nanoparticles for electrocatalytic oxidation of hydrazine in alkaline media,” *ACS Appl. Mater. Interfaces*, vol. 6, no. 21, pp. 18445–18449, 2014, doi: 10.1021/am5058635.

[123] S. S. Narwade, B. B. Mulik, S. M. Mali, and B. R. Sathe, “Silver nanoparticles sensitized C 60 (Ag@C 60) as efficient electrocatalysts for hydrazine oxidation: Implication for hydrogen generation reaction,” *Appl. Surf. Sci.*, vol. 396, pp. 939–944, 2017, doi: 10.1016/j.apsusc.2016.11.065.

[124] X. Yan, Y. Chen, M. Yang, Y. Shi, T. Gao, and Y. Li, “Efficient and Long-term Photoelectrochemical Hydrogen Liberation from Hydrazine Hydrate on CdS Nanorod Arrays,” *J. Electron. Mater.*, vol. 51, no. 6, pp. 3114–3124, 2022, doi: 10.1007/s11664-022-09559-x.

[125] N. Morlanés *et al.*, “A technological roadmap to the ammonia energy economy: Current state and missing technologies,” *Chem. Eng. J.*, vol. 408, no. August 2020, 2021, doi: 10.1016/j.cej.2020.127310.

[126] A. Di Carlo, A. Dell’Era, and Z. Del Prete, “3D simulation of hydrogen production by ammonia decomposition in a catalytic membrane reactor,” *Int. J. Hydrogen Energy*, vol. 36, no. 18, pp. 11815–11824, 2011, doi: 10.1016/j.ijhydene.2011.06.029.

[127] N. Itoh, Y. Kikuchi, T. Furusawa, and T. Sato, “Tube-wall catalytic membrane reactor for hydrogen production by low-temperature ammonia decomposition,” *Int. J. Hydrogen Energy*, vol. 46, no. 38, pp. 20257–20265, 2021, doi: 10.1016/j.ijhydene.2020.03.162.

[128] M. E. E. Abashar, “Multi-stage membrane reactors for hydrogen production by ammonia decomposition,” *Int. J. Petrochemistry Res.*, vol. 2, no. 1, pp. 109–115, 2018, doi: 10.18689/ijpr-1000120.

[129] J. L. Cerrillo *et al.*, “High purity, self-sustained, pressurized hydrogen production from ammonia in a catalytic membrane reactor,” *Chem. Eng. J.*, vol. 431, no. December

2021, 2022, doi: 10.1016/j.cej.2021.134310.

[130] V. Cechetto, L. Di Felice, R. Gutierrez Martinez, A. Arratibel Plazaola, and F. Gallucci, “Ultra-pure hydrogen production via ammonia decomposition in a catalytic membrane reactor,” *Int. J. Hydrogen Energy*, vol. 47, no. 49, pp. 21220–21230, 2022, doi: 10.1016/j.ijhydene.2022.04.240.

[131] S. Shwe Hla and M. D. Dolan, “CFD modelling of a membrane reactor for hydrogen production from ammonia,” *IOP Conf. Ser. Mater. Sci. Eng.*, vol. 297, no. 1, 2018, doi: 10.1088/1757-899X/297/1/012027.

[132] H. Cheng *et al.*, “Single-step synthesized dual-layer hollow fiber membrane reactor for on-site hydrogen production through ammonia decomposition,” *Int. J. Hydrogen Energy*, vol. 45, no. 12, pp. 7423–7432, 2020, doi: 10.1016/j.ijhydene.2019.04.101.

[133] Z. Zhang, S. Liguori, T. F. Fuerst, J. D. Way, and C. A. Wolden, “Efficient Ammonia Decomposition in a Catalytic Membrane Reactor to Enable Hydrogen Storage and Utilization,” *ACS Sustain. Chem. Eng.*, vol. 7, no. 6, pp. 5975–5985, 2019, doi: 10.1021/acssuschemeng.8b06065.

[134] S. Chiuta, R. C. Everson, H. W. J. P. Neomagus, P. Van Der Gryp, and D. G. Bessarabov, “Reactor technology options for distributed hydrogen generation via ammonia decomposition: A review,” *Int. J. Hydrogen Energy*, vol. 38, no. 35, pp. 14968–14991, 2013, doi: 10.1016/j.ijhydene.2013.09.067.

[135] Y. L. Chen, C. F. Juang, and Y. C. Chen, “The effects of promoter cs loading on the hydrogen production from ammonia decomposition using ru/c catalyst in a fixed-bed reactor,” *Catalysts*, vol. 11, no. 3, pp. 1–15, 2021, doi: 10.3390/catal11030321.

[136] Y. Gu, Y. Ma, Z. Long, S. Zhao, Y. Wang, and W. Zhang, “One-pot synthesis of supported Ni@Al2O3 catalysts with uniform small-sized Ni for hydrogen generation via ammonia decomposition,” *Int. J. Hydrogen Energy*, vol. 46, no. 5, pp. 4045–4054, 2021, doi: 10.1016/j.ijhydene.2020.11.003.

[137] N. Morlanés *et al.*, “Development of a Ba-CoCe catalyst for the efficient and stable decomposition of ammonia,” *Catal. Sci. Technol.*, vol. 11, no. 9, pp. 3014–3024, 2021, doi: 10.1039/d0cy02336a.

[138] F. Zhiqiang *et al.*, “Catalytic ammonia decomposition to COx-free hydrogen over

ruthenium catalyst supported on alkali silicates," *Fuel*, vol. 326, no. April, p. 125094, 2022, doi: 10.1016/j.fuel.2022.125094.

[139] I. Lucentini, G. García Colli, C. D. Luzi, I. Serrano, O. M. Martínez, and J. Llorca, "Catalytic ammonia decomposition over Ni-Ru supported on CeO2 for hydrogen production: Effect of metal loading and kinetic analysis," *Appl. Catal. B Environ.*, vol. 286, no. December 2020, 2021, doi: 10.1016/j.apcatb.2021.119896.

[140] I. Lucentini *et al.*, "Modelling and simulation of catalytic ammonia decomposition over Ni-Ru deposited on 3D-printed CeO2," *Chem. Eng. J.*, vol. 427, no. July 2021, 2022, doi: 10.1016/j.cej.2021.131756.

[141] L. A. Jolaoso *et al.*, "Ammonia decomposition over citric acid induced γ-Mo2N and Co3Mo3N catalysts," *Int. J. Hydrogen Energy*, vol. 43, no. 10, pp. 4839–4844, 2018, doi: 10.1016/j.ijhydene.2018.01.092.

[142] A. R. Kim *et al.*, "Hydrogen production from ammonia decomposition over Ru-rich surface on La2O2CO3-Al2O3 catalyst beads," *Catal. Today*, no. April, 2022, doi: 10.1016/j.cattod.2022.08.009.

[143] X. Vendrell, J. Llorca, and I. Lucentini, "Review of the Decomposition of Ammonia to Generate Hydrogen," 2021, doi: 10.1021/acs.iecr.1c00843.

[144] N. Engelbrecht, S. Chiuta, and D. G. Bessarabov, "A highly efficient autothermal microchannel reactor for ammonia decomposition: Analysis of hydrogen production in transient and steady-state regimes," *J. Power Sources*, vol. 386, no. February, pp. 47–55, 2018, doi: 10.1016/j.jpowsour.2018.03.043.

[145] K. Schumacher, N. Engelbrecht, R. C. Everson, M. Friedl, and D. G. Bessarabov, "Steady-state and transient modelling of a microchannel reactor for coupled ammonia decomposition and oxidation," *Int. J. Hydrogen Energy*, vol. 44, no. 13, pp. 6415–6426, 2019, doi: 10.1016/j.ijhydene.2019.01.132.

[146] K. Gyak, N. K. Vishwakarma, Y. Hwang, J. Kim, H. Yun, and D. Kim, "Reaction Chemistry & Engineering from a photocurable preceramic resin for the high temperature ammonia cracking process †," pp. 1393–1399, 2019, doi: 10.1039/c9re00201d.

[147] H. Maleki, M. Fulton, and V. Bertola, "Kinetic assessment of H2 production from

NH3 decomposition over CoCeAlO catalyst in a microreactor: Experiments and CFD modelling," *Chem. Eng. J.*, vol. 411, no. December 2020, p. 128595, 2021, doi: 10.1016/j.cej.2021.128595.

[148] C. Chen *et al.*, "Bimetallic Ru-Fe Nanoparticles Supported on Carbon Nanotubes for Ammonia Decomposition and Synthesis," *Chem. Eng. Technol.*, vol. 43, no. 4, pp. 719–730, 2020, doi: 10.1002/ceat.201900508.